Thesis for the degree of Doctor of Philosophy

Signaling for Optical Intensity Channels

JOHNNY KAROUT

CHALMERS

Communication Systems Group
Department of Signals and Systems
Chalmers University of Technology

Gothenburg, Sweden 2013

Karout, Johnny
Signaling for Optical Intensity Channels.

ISBN 978-91-7385-865-6
Doktorsavhandlingar vid Chalmers tekniska högskola
Ny serie Nr 3546
ISSN 0346-718X

Communication Systems Group
Department of Signals and Systems
Chalmers University of Technology
SE-412 96 Gothenburg, Sweden
Telephone: + 46 (0)31-772 1000

This thesis has been prepared using LaTeX.

Printed by Chalmers Reproservice,
Gothenburg, Sweden, July 2013.

To my beloved family

"Do not go where the path may lead, go instead where there is no path and leave a trail."
Ralph Waldo Emerson

Abstract

With the growing popularity of social media services, e-commerce, and many other internet-based services, we are witnessing a rapid growth in the deployment of data centers and cloud computing platforms. As a result, the telecommunications industry has to continue providing additional network capacity to meet the increasing demand for bandwidth. The use of fiber-optic communications plays a key role in meeting this demand. Coherent optical transceivers improve spectral efficiency by allowing the use of multilevel in-phase and quadrature (I/Q) modulation formats, which encode information onto the optical carrier's amplitude and phase. However, for short-haul optical links, using noncoherent optical transceivers, also known as intensity-modulated direct-detection (IM/DD) systems, is a more attractive low-cost approach. Since only the intensity of light can carry information, designing power- and spectrally-efficient modulation formats becomes challenging. Subcarrier modulation, a concept studied in wireless infrared communications, allows the use of I/Q modulation formats with IM/DD systems at the expense of power and spectral efficiency.

This thesis addresses the problem of optimizing single-subcarrier modulation formats for noncoherent fiber and wireless optical communication systems in order to achieve a good trade-off between spectral efficiency, power efficiency, and cost/complexity. For the single-subcarrier three-dimensional signal space, denoted as raised-QAM in the literature, we propose a set of 4-, 8-, and 16-level modulation formats which are numerically optimized for average electrical, average optical, and peak power. In the absence of error-correcting codes, the optimized formats offer gains ranging from 0.6 to 3 dB compared to the best known formats. However, when error-correcting codes with performance near capacity are present, the obtained modulation formats offer gains ranging from 0.3 to 1 dB compared to previously known formats. In addition, laboratory experiments using the obtained 4- and 8-ary modulation formats were carried out. The performance improvement over the previously known formats conforms with the theoretical results.

To address transceiver complexity, a two-dimensional signal space for optical IM/DD systems is proposed. The resulting modulation formats have simpler modulator and demodulator structures than the three-dimensional formats. Their spectra have in general narrower main lobes but slower roll-off, which make them a good choice for single-wavelength optical systems. The three-dimensional formats are more suitable for wavelength-division multiplexing systems, where crosstalk between adjacent channels is important.

Keywords: Direct detection, fiber-optical communications, free-space optical communications, infrared communications, intensity modulation, lattice codes, mutual information, noncoherent communications, sphere packing.

List of Included Publications

This thesis is based on the following publications:

Paper A

J. Karout, E. Agrell, and M. Karlsson, "Power efficient subcarrier modulation for intensity modulated channels," *Optics Express*, vol. 18, no. 17, pp. 17 913–17 921, Aug. 2010.

Paper B

K. Szczerba, **J. Karout**, P. Westbergh, E. Agrell, M. Karlsson, P. Andrekson, and A. Larsson, "Experimental comparison of modulation formats in IM/DD links," *Optics Express*, vol. 19, no. 10, pp. 9881–9889, May 2011.

Paper C

J. Karout, E. Agrell, K. Szczerba, and M. Karlsson, "Optimizing constellations for single-subcarrier intensity-modulated optical systems," *IEEE Transactions on Information Theory*, vol. 58, no. 7, pp. 4645–4659, Jul. 2012.

Paper D

K. Szczerba, **J. Karout**, E. Agrell, P. Westbergh, M. Karlsson, P. Andrekson, and A. Larsson, "Demonstration of 8-level subcarrier modulation sensitivity improvement in an IM/DD system," in *Proc. European Conference and Exhibition on Optical Communication*, 2011.

Paper E

J. Karout, G. Kramer, F. R. Kschischang, and E. Agrell, "Modulation method and apparatus for amplitude- or intensity-modulated communication systems," *U.S. Provisional Patent Application*, No. 61602104, filing date Feb. 23, 2012.

Paper F

J. Karout, G. Kramer, F. R. Kschischang, and E. Agrell, "A two-dimensional signal space for intensity-modulated channels," *IEEE Communications Letters*, vol. 16, no. 9, pp. 1361–1364, Sep. 2012.

List of Related Publications

Below are other contributions by the author that are not included in this thesis, either due to content overlap with the appended papers, or due to content that is outside the scope of this thesis.

Patent Applications

[P1] **J. Karout**, G. Kramer, F. R. Kschischang, and E. Agrell, "Modulation method and apparatus for amplitude- or intensity-modulated communication systems," U.S. Patent Application No. 13/491,655 (filing date Jun. 8, 2012).

[P2] **J. Karout**, K. Szczerba, and E. Agrell, "Modulation scheme," U.S. Patent Application No. 12/976,188, Publication No. 20110200337 (published Aug. 18, 2011).

[P3] **J. Karout**, K. Szczerba, and E. Agrell, "A novel subcarrier modulation scheme for the optical intensity channel," U.S. Provisional Patent Application No. 61304459 (filing date Feb. 14, 2010).

Journal Publications

[J1] M. Tavan, E. Agrell, and **J. Karout**, "Bandlimited intensity modulation," *IEEE Transactions on Communications*, vol. 60, no. 11, pp. 3429–3439, Nov. 2012.

[J2] K. Szczerba, P. Westbergh, **J. Karout**, J. S. Gustavsson, Å. Haglund, M. Karlsson, P. A. Andrekson, E. Agrell, and A. Larsson, "4-PAM for high-speed short-range optical communications," *Journal of Optical Communications and Networking*, vol. 4, no. 11, pp. 885–894, Nov. 2012.

[J3] K. Szczerba, P. Westbergh, **J. Karout**, J. Gustavsson, Å. Haglund, M. Karlsson, P. Andrekson, E. Agrell, and A. Larsson, "30 Gbps 4-PAM transmission over 200 m of MMF using an 850 nm VCSEL," *Optics Express*, vol. 19, no. 26, pp. B203–B208, Dec. 2011.

Conference Publications

[C1] **J. Karout**, X. Liu, S. Chandrasekhar, E. Agrell, M. Karlsson, and R.-J. Essiambre, "Experimental demonstration of an optimized 16-ary four-dimensional modulation format using optical OFDM," in *Proc. Optical Fiber Communication Conference*, 2013, paper OW3B.4.

[C2] **J. Karout**, G. Kramer, F. R. Kschischang, and E. Agrell, "Continuous-amplitude modulation for optical wireless channels," in *Proc. IEEE Photonics Society Summer Topical Meetings*, Jul. 2012, paper WB4.4.

[C3] K. Szczerba, **J. Karout**, M. Karlsson, P. Andrekson, and E. Agrell, "Optimized lattice-based 16-level subcarrier modulation for IM/DD systems," in *Proc. European Conference and Exhibition on Optical Communication*, 2012.

[C4] **J. Karout**, E. Agrell, K. Szczerba, and M. Karlsson, "Designing power-efficient modulation formats for noncoherent optical systems," in *Proc. IEEE Global Communications Conference*, 2011. **(Best Paper Award)**

[C5] M. Tavan, E. Agrell, and **J. Karout**, "Strictly bandlimited ISI-free transmission over intensity-modulated channels," in *Proc. IEEE Global Communications Conference*, 2011.

[C6] K. Szczerba, P. Westbergh, J. Gustavsson, Å. Haglund, **J. Karout**, M. Karlsson, P. Andrekson, E. Agrell, and A. Larsson, "30 Gbps 4-PAM transmission over 200m of MMF using an 850 nm VCSEL," in *Proc. European Conference and Exhibition on Optical Communication*, 2011.

[C7] N. Jiang, Y. Gong, **J. Karout**, H. Wymeersch, P. Johannisson, M. Karlsson, E. Agrell, and P. A. Andrekson, "Stochastic backpropagation for coherent optical communications," in *Proc. European Conference and Exhibition on Optical Communication*, 2011.

[C8] **J. Karout**, H. Wymeersch, A. S. Tan, P. Johannisson, E. Agrell, M. Sjödin, M. Karlsson, and P. Andrekson, "CMA misconvergence in coherent optical communication for signals generated from a single PRBS," in *Proc. Wireless and Optical Communications Conference*, 2011.

[C9] **J. Karout**, L. S. Muppirisetty, and T. Svensson, "Performance trade-off investigation of B-IFDMA," in *Proc. IEEE Vehicular Technology Conference*, Fall 2009.

Acknowledgements

Life is like a book! And here I am writing my last page of an important chapter, a chapter full of adventures to tell and stories to remember. Many people took part in it, and now it is my chance to thank each and every person without whom this chapter would not have been an interesting one.

First and foremost, I would like to express my deepest gratitude to my supervisor, Prof. Erik Agrell. Not only are you a great supervisor, but a great teacher too! Every day was a learning experience, and with your enthusiasm for research and your optimism, you have made my journey a fabulous one. Thank you! I would also like to thank my co-supervisor, Prof. Magnus Karlsson, for all the motivation and support he has provided. It was such a pleasure working with you!

I am very grateful to Prof. Gerhard Kramer and Prof. Frank R. Kschischang for their support and all the nice discussions we had. You both made me think outside the box, and working with you has been such a wonderful experience! I would like to thank Dr. René-Jean Essiambre and Dr. Xiang Liu for involving me in many interesting research topics. You both taught me that dedication and persistence are key ingredients for things to happen. I would also like to thank Dr. Bruce Moision for all the support and encouragement he has provided. It has been great to work with you.

I would like to thank each and every member of the fiber optic communications research center (FORCE) for making it such a nice research environment. A special thanks goes to Associate Prof. Henk Wymeersch and Assistant Prof. Pontus Johannisson for their motivation, support, and all the new research topics they introduced me to. I would also like to thank Krzysztof Szczerba for all the nice discussions we had. It was a pleasure working with you.

Many thanks to Prof. Erik Ström for all his efforts to make the

experience of being in the Communication Systems Group an interesting one. I would like to thank Prof. Arne Svensson, Prof. Thomas Eriksson, Associate Prof. Tommy Svensson, Dr. Mats Rydström, Assistant Prof. Giuseppe Durisi, Assistant Prof. Fredrik Brännström, Assistant Prof. Alexandre Graell i Amat, Associate Prof. Lennart Svensson, Assistant Prof. Michail Matthaiou, Dr. Guillermo Garcia, Dr. Arash Tahmasebi, and Dr. Alex Alvarado for all the nice discussions. Thanks to Dr. Ali Soltani, Dr. Nima Seifi, Kasra Haghighi, Srikar Muppirisetty, Lotfollah Beygi, Christian Häger, Mikhail Ivanov, Mohammad Reza Gholami, Tilak Rajesh Lakshmana, M. Reza Khanzadi, and Rajet Krishnan for all the short discussions on life experiences. I would also like to thank the current and former members of the group. Many thanks to Agneta, Natasha, and Lars for all their help. It is difficult to imagine the department without all of you. Special thanks goes to Livia, Giota, Astrid, Antonia, Jaime, Elena, Karin, Tomas, Johan, Walid, and Luca for being great friends! A big thank you goes to my Aikido family in Gothenburg for all the pleasant time we have spent together.

My sincerest gratitude and love goes to my family for all the support they have given me over the years. Mom, you have always been a great source of inspiration and encouragement. A thank you is just not enough! Brothers, although each had and still has his own way of support, I owe you all a big thank you. Simon, you always manage to put a smile on people's faces. Peter, you know how to take good care of the people surrounding you. Roger, you make the impossible possible. I am really lucky to have you all! Finally, a special thank you goes to my only sister Randa. You have been a great source of support, motivation, and inspiration!

Johnny Karout
Gothenburg, June 2013

Thanks to SSF and the Swedish Research Council for supporting this work under grants RE07-0026 and 2010-5757, respectively. In addition, thanks to LINDO Systems for the free license to use their numerical optimization software.

Contents

Acronyms

AB-QAM	Adaptively-Biased QAM
ASK	Amplitude-Shift Keying
AWG	Arbitrary Waveform Generator
AWGN	Additive White Gaussian Noise
BPSK	Binary Phase-Shift Keying
DC	Direct Current
FDM	Frequency Division-Multiplexing
IM/DD	Intensity-Modulated Direct-Detection
I/Q	In-phase and Quadrature
LED	Light-Emitting Diode
LO	Local Oscillator
LPF	Low-Pass Filter
MAP	Maximum A Posteriori
MF	Matched Filter
ML	Maximum Likelihood
MMF	Multimode Fiber
M-PAM	M-ary Pulse Amplitude Modulation
M-PPM	M-ary Pulse-Position Modulation
M-PSK	M-ary Phase-Shift Keying

M-QAM	M-ary Quadrature Amplitude Modulation
MSM	Multiple-Subcarrier Modulation
MZM	Mach–Zehnder Modulator
OFDM	Orthogonal Frequency-Division Multiplexing
OOK	On-Off Keying
PDM-QPSK	Polarization-Division Multiplexed QPSK
QPSK	Quadrature Phase-Shift Keying
RIN	Relative Intensity Noise
SCM	Subcarrier Modulation
SER	Symbol Error Rate
SNR	Signal-to-Noise Ratio
VCSEL	Vertical-Cavity Surface-Emitting Laser
VLC	Visible Light Communication
VOA	Variable Optical Attenuator

Part I

Introduction

Chapter 1

Overview

Over the past few decades, there have been significant technological advancements that have paved the way for the *information* or *digital era* we are living in. With the growing popularity of social media services, e-commerce, and many other internet-based services, we are witnessing a rapid growth in the deployment of data centers, storage area networks, and cloud computing platforms. As a result, the telecommunications industry has to continue providing additional network capacity to meet the increasing demand for bandwidth. In 1948, Claude Elwood Shannon, with his landmark paper titled "A mathematical theory of communication" [1], established the theory that deals with the fundamental limits of storing and communicating data. It is what he called *information theory*. This theory can be used as a benchmark for any communication system. Since then, efforts have been devoted to designing communication systems that provide a good trade-off between spectral efficiency, power efficiency, and cost/complexity, as shown in Fig. 1.1.

The earliest methods of communicating between a sender and a remote receiver used acoustic or optical communications. In the *Iliad* by Homer, it was mentioned that fire beacons were used to transmit information in the siege of Troy, which took place in approximately 1184 BC [2, Sec. 1.1]. However, it was not until the invention of the laser in the late 1950s that optical communication was realized the way we know it today [3, Ch. 1]. Since then, a lot of experiments have investigated the different methods of guiding light, until the breakthrough by Kao and Hockham in 1966, whereby they proposed

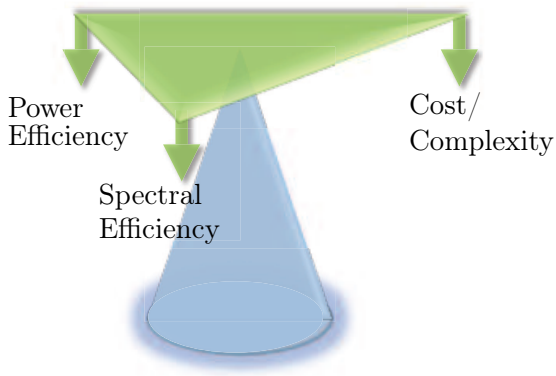

Figure 1.1: Trade-offs in the design of a communication system.

the use of silica glass fibers [4]. Together with the further development of low-loss single-mode fibers [5], long-haul fiber-optic transmission became feasible. Today, a massive network of fiber optic cables exists worldwide [3, Sec. 1.1]. For long transmission distances, the overall costs are shared among many users. Therefore, it is feasible to deploy coherent optical communication systems (see Sec. 3.1) that enable high spectral efficiency by encoding information on the amplitude and phase in both polarizations of the optical carrier.

On the contrary, short-haul optical communication systems are more cost constrained. Such links are not often shared among many users, therefore, it is tricky to bring their costs down. Examples of such types of communication systems include wireless optical communications [2, 6, 7] and short-haul fiber links prevalent in local area networks, storage area networks, high-performance computing, and data centers [8–11]. Typically, multimode fibers (MMF) are used in these applications since they are more alignment tolerant in comparison to single-mode fibers, which results in lower installation costs. In addition, affordable optics such as noncoherent optical transceivers are required to meet the cost constraints. These include vertical-cavity surface-emitting lasers (VCSELs), light-emitting diodes (LEDs), and direct-detection receivers in which a photodetector outputs an electrical signal proportional to the optical intensity. As opposed to coherent communications, noncoherent optical transceivers allow only

the intensity of the optical carrier to convey information and the square of the envelope of the received signal to be detected at the receiver. This type of noncoherent optical systems is known as *intensity-modulated direct-detection* (IM/DD) systems. IM/DD systems have fewer degrees of freedom compared to coherent communication systems. This reduces the flexibility in designing IM/DD links that provide a good trade-off between spectral efficiency, power efficiency, and cost/complexity.

In the absence of optical amplification, an IM/DD system can be modeled as a conventional additive white Gaussian noise (AWGN) channel whose input is constrained to being real and nonnegative [6, Ch. 5], [7, 12–15]. A simple approach to increase the spectral efficiency of IM/DD links beyond that of the widespread on-off keying (OOK) is to use M-ary pulse amplitude modulation (M-PAM). This is different from the conventional PAM since no negative amplitudes can be used [6, Eq. (5.8)]. The increased spectral efficiency of M-PAM comes at the expense of power efficiency, which was shown to be low in [16]. Another option is to use M-ary pulse-position modulation (M-PPM) formats. Such modulation formats increase the power efficiency, however, they suffer from poor spectral efficiency [6, Sec. 5.3.3], [7, 17].

Any real nonnegative electrical waveform can be successfully communicated over an IM/DD link. This implies that if the information is modulated on an electrical subcarrier using any M-level modulation format, it can be transmitted as the intensity of an optical carrier on an IM/DD link after adding a direct current (DC) bias to ensure its nonnegativity. The subcarrier amplitude and phase carry the information, and both will be retrieved at the receiver. This concept is known as *subcarrier modulation* (SCM) and was described in the wireless infrared communications context [6, Ch. 5]. SCM is an alternative approach that allows the use of higher-order modulation formats with IM/DD systems that are more power efficient than M-PAM. As for the conventional electrical channel, many subcarriers can be superimposed resulting in a frequency division-multiplexing (FDM) system, referred to as multiple-subcarrier modulation (MSM) in the wireless infrared context [6, p. 122], and orthogonal frequency-division multiplexing (OFDM) if the carriers are orthogonal [18]. In [6, Sec. 5.3.2] and [19], MSM was shown to have poor power efficiency compared to

single-subcarrier modulation.

For single-subcarrier modulation formats, one option is that the DC bias required to ensure the nonnegativity of the electrical waveform does not carry information [6, Ch. 5], [20, 21]. The second option is to allow the DC bias to carry information, thus potentially improving the power efficiency. This was studied by varying the DC bias on a symbol-by-symbol basis in [22] and within the symbol interval in [23]. In [13], Hranilovic presented the first signal space analysis for optical IM/DD channels, and derived shaping regions to reduce the average and peak optical power. These regions were used to construct power-efficient lattice-based modulation formats that are characterized by their regular geometric structure, thus reducing the complexity of the transceiver.

In this work, we address the problem of optimizing single-subcarrier modulation formats for uncoded IM/DD systems, with and without confining them to a lattice structure, in order to achieve a good trade-off between spectral efficiency, power efficiency, and cost/complexity. For the three-dimensional signal space for IM/DD, whose signal sets are denoted as raised-QAM [13], we propose a set of 4-, 8-, and 16-level single-subcarrier modulation formats which are numerically optimized for average electrical, average optical, and peak power. These optimization criteria are all relevant since they help in assessing the power consumption in optical communications [24], the conformity to skin- and eye-safety measures in wireless optical links [6, Ch. 5], [7, 13], and the tolerance against the nonlinearities present in the system [25] (see Chapter 4 for details). In addition, laboratory experiments were carried out to see to what degree the experimental results differed from the theory. We then analyze the obtained modulation formats in terms of mutual information at different signal-to-noise ratios (SNR), in order to predict their performance in the presence of strong error-correcting codes. Further, we analytically optimize modulation formats in the wideband regime, i.e., at low SNR, and compare them with other formats. To address transceiver complexity, we propose a family of two-dimensional signal spaces for IM/DD channels which can be used to construct modulation formats. Among this family of signal spaces, we choose a two-dimensional signal space that is a subspace of the three-dimensional raised-QAM signal space to optimize modulation formats for the different power measures. We then eval-

uate the power and spectral efficiencies of those modulation formats and compare them to the previously best known formats.

This thesis is organized as follows. Chapter 2 presents the signal space analysis in digital communications as well as the use of sphere packing to design power-efficient modulation formats. Chapter 3 introduces the system models of coherent and noncoherent optical communications. Chapter 4 focuses on single-subcarrier modulation formats for IM/DD channels. The three-dimensional raised-QAM signal space is presented. Then, the two-dimensional signal space is introduced together with the figures of merit and an example of optimized modulation formats. Finally, in Chapter 5, the contributions are summarized.

Chapter 2

Digital Communications

The earliest form of electrical communication was digital with the invention of telegraphy by Samuel Morse in 1837 [26, Ch. 1]. Even with this early form of communication, source coding was used since frequent letters of the English alphabet were represented by short sequences of dots and dashes, and less frequent letters were represented by longer sequences. It took almost a century to realize digital communications the way we know it today. This started with the work of Nyquist in 1924, who investigated the maximum rates that can be used over a bandlimited telegraph channel without intersymbol interference [27]. Then followed the work of Hartley in 1928, who investigated the maximum rates that can be achieved over a bandlimited channel in the presence of a fixed power constraint [28]. Another milestone was the work of Wiener in 1942, where he investigated the problem of estimating the desired signal at the receiver in the presence of additive noise [29]. Then followed the work of Shannon and his landmark paper titled "A mathematical theory of communication" in 1948 [1]. Shannon established the mathematical foundations for information transmission and derived the fundamental limits of digital communication systems, given by the *channel capacity*. This capacity gives the highest rate in bits per channel use at which information can be sent with arbitrarily low error probability. Since then, the channel capacity and its underlying theory have served as a benchmark for all the new advances in the area of digital communications.

This chapter focuses on the classical AWGN channel model. Section 2.1 introduces the concept of *signal space* that provides an ele-

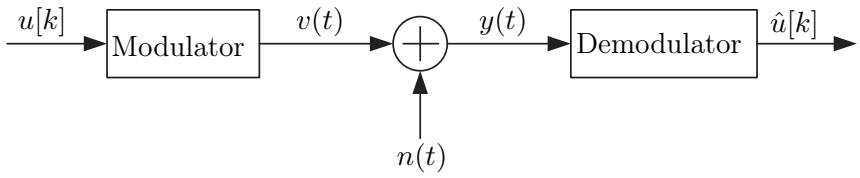

Figure 2.1: The model of a communication system.

gant way to analyze a communication system. This will be the basis for understanding the specific class of in-phase and quadrature (I/Q) modulation formats such as M-ary phase-shift keying (M-PSK) and quadrature amplitude modulation (M-QAM). Section 2.2 presents the I/Q modulator and the two classes of demodulation, coherent and noncoherent. The former has complete knowledge of the carrier phase, and the latter has no carrier phase knowledge. Finally, Sec. 2.3 introduces sphere packing and how it is used to design power-efficient modulation formats.

2.1 Signal Space Analysis

Consider the schematic of a communication system depicted in Fig. 2.1. It consists of a modulator that maps a symbol $u[k]$ at instant k to a waveform $v(t)$ belonging to the signaling set $S = \{s_0(t), s_1(t), \ldots, s_{M-1}(t)\}$, where M is the size of the signaling set. In this section, we will only consider the transmission of a single symbol. The generated waveform $v(t)$ propagates through the transmission medium, and the signal at the receiver can be written as

$$y(t) = v(t) + n(t), \tag{2.1}$$

where $n(t)$ is a zero-mean Gaussian process with double-sided power spectral density $N_0/2$ which can model the thermal noise generated at the receiver. The demodulator is a correlator or matched filter receiver with a minimum-distance detector, i.e., it minimizes the symbol error rate (SER) at a given SNR [30, Sec. 4.1] and puts out $\hat{u}[k]$, the symbol that was most likely sent.

By using the signal space analysis developed by Kotelnikov [31], and later expanded by Wozencraft and Jacobs [32], the continuous-time signals can be portrayed as points in Euclidean space. This

provides an insight into the detection methods and the performance of the various signaling schemes. In addition, viewing the signaling set as a constellation of points in Euclidean space provides a better understanding and an intuition on how to better design such signaling sets.

Consider a set of orthonormal basis functions $\phi_k(t)$ for $k = 1, 2, \ldots, N$ and $N \leq M$ such that each of the signals in S can be represented as

$$s_i(t) = \sum_{k=1}^{N} s_{i,k}\phi_k(t), \tag{2.2}$$

for $i = 0, \ldots, M-1$. The N-dimensional vector representation of $s_i(t)$ with respect to these basis functions is $\mathbf{s}_i = (s_{i,1}, s_{i,2}, \ldots, s_{i,N})$. Therefore, the constellation representing the M-ary signaling set S can be written as $\Omega = \{\mathbf{s}_0, \mathbf{s}_1, \ldots, \mathbf{s}_{M-1}\}$. In a similar fashion, the noise $n(t)$ can be expressed as

$$n(t) = \sum_{k=1}^{N} n_k\phi_k(t) + w(t), \tag{2.3}$$

where $w(t)$ is the noise component outside the space spanned by the basis functions $\phi_1(t), \ldots, \phi_N(t)$, which all the signals in S belong to. However, according to the *Theorem of Irrelevance*, the noise outside the dimensions of the signals has no effect on the detection process [33, p. 52]. Therefore, without loss of generality, the vector representation of the noise component that affects the detection process is

$$\mathbf{n} = (n_1, n_2, \ldots, n_N). \tag{2.4}$$

The continuous-time model in (2.1) can then be represented by the discrete-time vector model

$$\mathbf{y} = \mathbf{v} + \mathbf{n}, \tag{2.5}$$

where $\mathbf{v} \in \Omega$ is the transmitted vector, and $\mathbf{n}$ is a Gaussian random vector with independent elements, zero mean, and variance $N_0/2$ per dimension. The received vector $\mathbf{y} = (y_1, y_2, \ldots, y_N)$ is computed in the demodulator by a bank of correlators or matched filters as

$$y_j = \int_{-\infty}^{\infty} y(t)\phi_j(t)\,\mathrm{d}t, \qquad j = 1, 2, \ldots, N. \tag{2.6}$$

The optimum detector is based on the maximum a posteriori (MAP) criterion or the maximum likelihood (ML) criterion when the transmitted signals are equally probable [33, Sec. 2.5.1]. Therefore, using the signal space analysis and the fact that the noise is AWGN, it can be realized that this detector outputs the signal vector in Ω that is closest in Euclidean distance to the received signal vector $\mathbf{y}$. Equivalently, the Voronoi diagram of a modulation format can be used, where a decision region is constructed for each of the constellation points. Therefore, the detector decides on a specific symbol if the received vector falls in the corresponding decision region.

2.2 I/Q Modulation and Demodulation

The widespread I/Q modulation formats such as M-PSK and M-QAM give access to both the electrical carrier's amplitude and phase to carry information. These I/Q modulation formats can be portrayed in a two-dimensional Euclidean space spanned by the orthonormal basis functions [33, Sec. 3.2.3]

$$\phi_1(t) = \sqrt{2}\, p(t) \cos(2\pi f t), \tag{2.7}$$
$$\phi_2(t) = \sqrt{2}\, p(t) \sin(2\pi f t), \tag{2.8}$$

where f is the carrier frequency, and $p(t)$ is a unit-energy baseband pulse, i.e., $\int_{-\infty}^{\infty} p^2(t)\,\mathrm{d}t = 1$.

2.2.1 Orthonormality Criterion

An orthonormal set of basis functions is convenient for the signal space analysis in Sec. 2.1, and a necessity for the optimality of minimum-distance detection. The orthonormality criterion is satisfied if the basis functions have unit energies and are orthogonal to each other such that

$$\int_{-\infty}^{\infty} \phi_n(t)\phi_m(t)\,\mathrm{d}t = \begin{cases} 1, & m = n, \\ 0, & m \neq n. \end{cases}$$

The orthogonality of (2.7) and (2.8) is guaranteed if the pulse $p(t)$ has bandwidth $W < f$. In practical applications, a strictly bandlimited pulse is difficult to generate. By using $f \gg 1/T_s$, where T_s is the

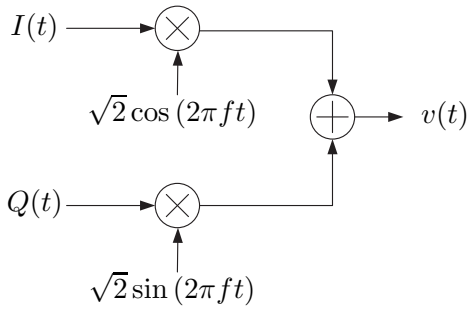

Figure 2.2: I/Q modulator.

symbol period, near orthogonality can be achieved regardless of $p(t)$. However, if $p(t)$ is a rectangular pulse for $0 < t \leq T_s$, the orthogonality criterion can still be satisfied if f is a multiple of $1/T_s$. This idea is used in OFDM for the subcarrier spacing, and for the subcarrier modulation formats that will be discussed in Chapter 4.

2.2.2 Modulator

Figure 2.2 depicts the setup of an I/Q modulator, where a pulse train is sent as opposed to restricting the transmission to a single symbol as in Sec. 2.1. The symbols $u[k]$, for $k = \ldots, -1, 0, 1, \ldots$, are independent and uniformly distributed over $\{0, 1, \ldots, M-1\}$. The in-phase and quadrature baseband pulse trains

$$I(t) = \sum_k s_{u[k],1}\ p(t - kT_s)$$

and

$$Q(t) = \sum_k s_{u[k],2}\ p(t - kT_s)$$

are multiplied by $\sqrt{2}\cos(2\pi ft)$ and $\sqrt{2}\sin(2\pi ft)$, respectively. The sum of these two branches yields the passband transmitted waveform

$$v(t) = \sqrt{2}[I(t)\cos(2\pi ft) + Q(t)\sin(2\pi ft)], \tag{2.9}$$

where information is carried on its amplitude and phase.

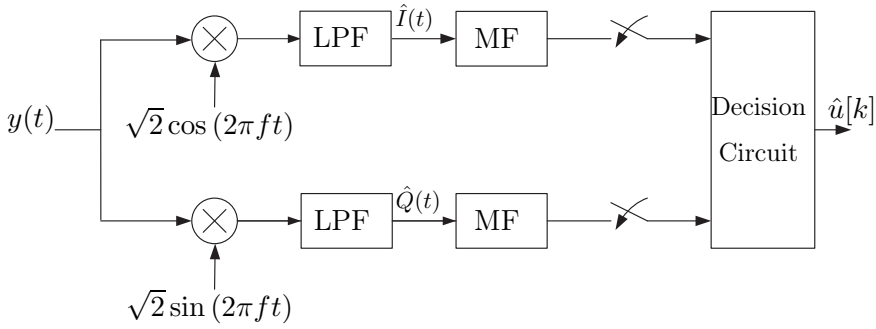

Figure 2.3: Coherent I/Q demodulator.

2.2.3 Demodulator

Assuming perfect carrier and symbol synchronization, the receiver can make use of the phase reference information to demodulate the received signal. This is known as coherent demodulation and is shown in Fig. 2.3. The receiver mixes the noisy received signal $y(t) = v(t)+n(t)$ with $\sqrt{2}\cos(2\pi ft)$ and $\sqrt{2}\sin(2\pi ft)$, i.e., the in-phase and quadrature sinusoidal references, generated by a local oscillator (LO) at the receiver. This is followed by low-pass filtering (LPF) that cancels the signal alias at twice the carrier frequency and outputs $\hat{I}(t)$ and $\hat{Q}(t)$, which are the estimates of the baseband signals $I(t)$ and $Q(t)$. These are fed to filters matched to the pulse $p(t)$, denoted as MF, which is then followed by sampling and a decision circuit that outputs the symbols closest in signal space to the received ones.

In some systems, carrier synchronization might be imperfect or not available at the receiver. For example, this can be due to implementation cost and complexity, LO phase noise, or the channel itself if it induces a time-varying phase. As a result, crosstalk between the in-phase and quadrature arms will arise [30, p. 309]. In such scenarios, noncoherent detection, where the receiver makes no use of the phase reference, is an attractive approach (see Sec. 3.2 for the case where the transmitter cannot use the carrier phase to convey information). For each $i = 0, 1, \ldots, M-1$, the optimum demodulator that minimizes the SER at a given SNR correlates the received signal $y(t)$ with $s_i(t)$ and a 90° phase-shifted version of $s_i(t)$ over the symbol period [34, Sec. 6.6]. The metric for signal i is obtained by

adding the squares of these two correlations, and the signal resulting in the largest metric is the optimum choice. This type of demodulator is suitable, for example, when frequency-shift keying formats are deployed. However, if the signals being transmitted are the same but differ with a phase shift, e.g., M-PSK formats, the resulting metrics are the same. This causes ambiguity at the receiver on which signal to decide upon. Such ambiguity can be resolved by using differential encoding, but that is outside the scope of this work.

2.3 Sphere Packing

A good metric for evaluating different modulation formats is the symbol error rate. However, it is sometimes challenging to compute the exact SER depending on the constellation geometry, number of levels, and number of dimensions. Therefore, the standard union bound, which is based on the pairwise error probabilities, can be used to upperbound the SER [30, Eq. (4.81)]. This union bound on the SER can be expressed as

$$P_s \leq \frac{1}{M} \sum_{i=0}^{M-1} \sum_{\substack{j=0 \\ j \neq i}}^{M-1} \mathrm{Q}\left(\frac{\|\mathbf{s}_i - \mathbf{s}_j\|}{\sqrt{2N_0}} \right), \tag{2.10}$$

and it serves as an accurate approximation of the SER at high SNR. It can be seen from (2.10) that in the high SNR regime, the errors will be dominated by the signals in Ω that are closest to each other. Therefore, the union bound can be approximated by

$$P_s \approx \frac{2K}{M} \, \mathrm{Q}\left(\frac{d_{\min}}{\sqrt{2N_0}} \right), \tag{2.11}$$

where K is the number of distinct pairs $(\mathbf{s}_i, \mathbf{s}_j)$ with $i < j$ for which $\|\mathbf{s}_i - \mathbf{s}_j\| = d_{\min}$, $d_{\min}$ is the minimum distance of the constellation, and $\mathrm{Q}(x) = 1/\sqrt{2\pi} \int_x^\infty \exp(-u^2/2)\,\mathrm{d}u$ is the Gaussian Q-function. This approximation approaches the true SER at high SNR. From (2.11), it can be inferred that a good modulation format is one which minimizes the energy, whether average or peak, while keeping $d_{\min}$ constant.

The design of asymptotic power-efficient modulation formats can be reformulated as a sphere-packing problem with the attempt of

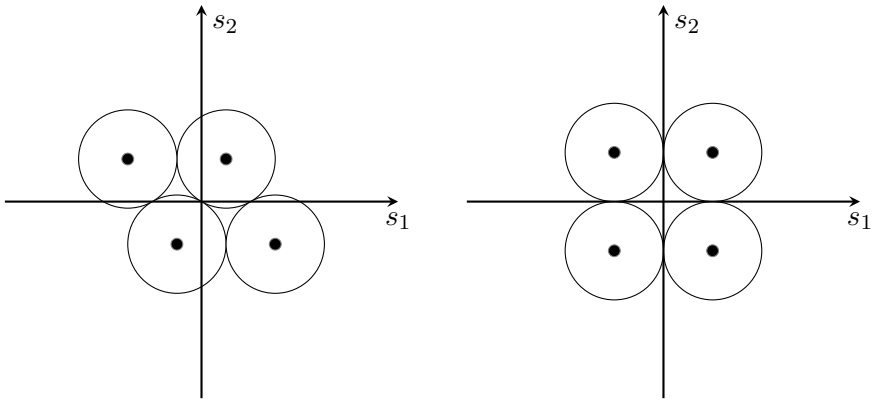

Figure 2.4: 4-level constellation optimized for average energy (left), and for average and peak energy simultaneously (right).

finding the densest packing of M N-dimensional spheres, e.g., two-dimensional for I/Q modulation formats. The coordinates of the sphere centers represent the constellation points. If the average energy

$$E_s = \frac{1}{M} \sum_{i=0}^{M-1} \|\mathbf{s}_i\|^2,$$

assuming that each symbol in the set is transmitted with the same probability, is the limiting factor in a communication system, then the objective would be to find the packing that minimizes the average squared distance of the center of the spheres from the origin. Other criteria for the optimization of sphere packings are discussed in Sec. 4.3 and [35–39].

Such problems can be well formulated mathematically, however, it is rather difficult to obtain an analytical solution. Therefore, numerical optimization techniques are used to find the best possible packing. This has been explored extensively for the AWGN channel with coherent detection for different power constraints, whether average or peak power [35–39]. The drawback is often the lack of geometric regularity, which increases the modulator and demodulator complexity. On the other hand, *lattice codes*, which are a finite set of points selected out of an N-dimensional lattice, is another approach that has

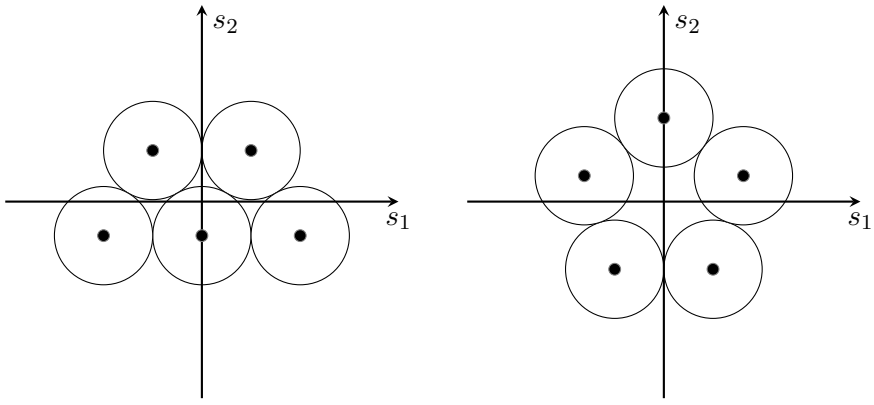

Figure 2.5: 5-level constellation optimized for average energy (left), and for peak energy (right).

been extensively used in the construction of multilevel modulation formats [40–42]. This approach might not guarantee optimality, however, it simplifies the modulator and demodulator due to the regular structure of a lattice.

2.3.1 Examples of Two-Dimensional Packings

In a two-dimensional signal space as the one presented in Sec. 2.2, the best known packing in terms of minimum average energy is, with one exception, a subset of the hexagonal lattice as shown in [38], whereas the packings optimized for the minimum peak energy have more irregular structures as can be found in [43]. The exception to this is shown in Fig. 2.4, where the two 4-level constellations presented have the same minimum average energy [38] among other possible constellations, despite the fact that the quadrature phase-shift keying (QPSK) constellation in Fig. 2.4 (right) is not a subset of the hexagonal lattice. However, the QPSK constellation offers the lowest peak energy for $M = 4$. On the other hand, Fig. 2.5 shows two 5-level constellations where the hexagonal lattice-based constellation (left) is optimized for average energy, and the constellation whose points lie on a circle is optimized for peak energy [44].

Chapter 3

Optical Communications

Optical communications, where fire beacons are used to convey information, date back to approximately 1184 BC [2, Sec. 1.1]. Since then, some of the key milestones the optical communications technology has passed through are the inventions of the optical telegraph by Chappe in the 1790s, the photophone by Bell and Tainter in the 1880s, and the laser in the late 1950s [2, Sec. 1.1]. Another key milestone is the silica fiber proposed by Kao and Hockham in 1966 [4]. This breakthrough in guiding light made long-haul transmission feasible, especially with the design of low-loss single-mode fibers. Today, the whole world is interconnected via a massive network of fiber optic cables [3, Sec. 1.1]. In addition, the growing popularity of data centers and cloud computing platforms is driving the demand for high-bandwidth short-haul optical links [11, 45]. In 1979, wireless optical communication was pioneered by Gfeller and Bapst with the use of diffuse emissions in the infrared band [46]. Nowadays, there is an increasing interest in wireless optical technologies such as visible light communication (VLC) [47–50]. This interest is due to the rapid deployment of energy-efficient LEDs, which are replacing incandescent and fluorescent lamps. Besides illumination, these LEDs are capable of utilizing the unlicensed visible light spectrum to transmit information. Other features of optical wireless communications include frequency reuse and improved security, since light is confined within the room it illuminates.

This chapter introduces coherent optical communications, which give access to both the amplitude and phase of the optical carrier.

The design of modulation formats is very similar to that of the AWGN channel presented in the previous chapter. Then follows the description of noncoherent optical communications, where information is transmitted only on the intensity of the optical carrier. The design of signaling schemes for noncoherent optical systems will be covered in depth in the following chapter.

3.1 Coherent Optical Communications

Coherent optical transceivers are prevalent in metro and long-haul optical systems. They give access to both quadratures in the two polarizations of the electromagnetic field for data transmission. Therefore, by using all the four degrees of freedom to transmit information, higher spectral efficiencies can be achieved [51–54]. For example, modulation formats such as OOK and binary phase-shift keying (BPSK) use only one degree of freedom, whereas I/Q modulation formats such as QPSK use two degrees of freedom. In order to use all the four degrees of freedom, I/Q modulation formats in the two polarizations should be used. An example of such a modulation format is the polarization-division multiplexed QPSK (PDM-QPSK), which has been extensively studied due to its ease of implementation [55].

A coherent transmitter consists of a light source and an external optical modulator. There are many possible structures to realize such an optical modulator [56]. One example is when the optical modulator block consists of both an amplitude and a phase modulator in series. Another example is by using an I/Q modulator with orthogonal optical carriers on the two arms, where each arm consists of an amplitude modulator such as a Mach–Zehnder modulator (MZM), and the transmitted signal is the combined output of the two arms. The receiver in general consists of photodetectors, an LO, and an electrical demodulator. The LO generates the in-phase and quadrature reference signals, which are mixed with the incoming light signal, and the output is sent to the photodetectors. The resulting photocurrents are used to reconstruct the electrical in-phase and quadrature components, which are further processed to extract the information bits that were transmitted.

The coherent optical channel, including optical amplifiers that introduce noise in the optical domain, can be modeled as an AWGN

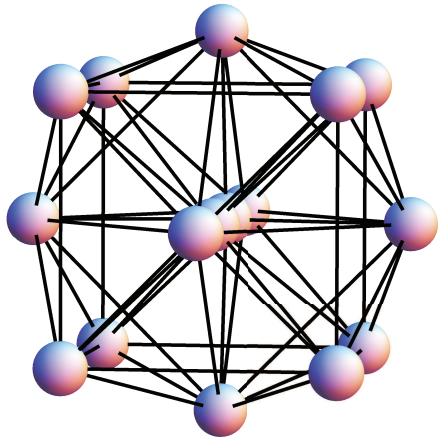

Figure 3.1: A projection of the best known 16-ary four-dimensional constellation $\mathscr{C}_{4,16}$ (from [61]).

channel in the absence of fiber nonlinearity [57–60]. Therefore, the problem of optimizing constellations to provide a good trade-off between power and spectral efficiency can be formulated as a sphere-packing problem [35–38]. The minimum distance between the spheres, i.e., the sphere diameter, governs the error rate performance at high SNR. As a result, all the theory obtained for the conventional electrical AWGN channel can be applied for coherent optical communications.

Specifically, the problem of optimizing modulation formats for coherent optical systems in a four-dimensional space, i.e., the two quadratures in both polarizations, has been thoroughly investigated in [39, 51–54, 61]. At a fixed spectral efficiency, designing more power-efficient formats, in the average energy sense, allows the transmitter to operate at a lower optical power, thereby mitigating the effect of nonlinear fiber transmission impairments. In signal space, the constellation set of PDM-QPSK consists of 16 symbols that lie on the vertices of a four-dimensional cube, thus providing 4 bits/symbol. The four-dimensional spheres with centers lying on the vertices of a cube do not provide the best packing in a four-dimensional Euclidean space. Consequently, there exist constellations providing a better power efficiency compared to PDM-QPSK while achieving the same error rate

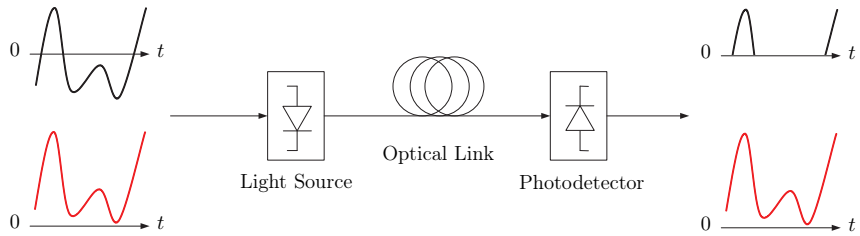

Figure 3.2: The black (top) and red (bottom) signals are to be transmitted over an IM/DD channel. The red signal is nonnegative and can therefore be transmitted successfully, as opposed to the black signal, which is clipped.

performance. In [61], a 16-ary four-dimensional constellation denoted as $\mathscr{C}_{4,16}$ was presented as the best known packing, in the average energy sense, of sixteen four-dimensional spheres. A projection of this constellation is depicted in Fig. 3.1. It can be described as a single point, six points lying on the vertices of a three-dimensional octahedron, eight points lying on the vertices of a three-dimensional cube, and another single point, all layered along one coordinate [61]. Its coordinate representation is $\mathscr{C}_{4,16} = \{(a+\sqrt{2},0,0,0),(a,\pm\sqrt{2},0,0),(a,0,\pm\sqrt{2},0),(a,0,0,\pm\sqrt{2}),(a-c,\pm1,\pm1,\pm1),(a-c-1,0,0,0)\}$ with all combinations of signs, where $a = (1-\sqrt{2}+9c)/16$ and $c = \sqrt{2\sqrt{2}-1}$. This constellation provides a 1.11 dB asymptotic average optical power gain over PDM-QPSK for the same spectral efficiency. In [62], we experimentally demonstrated the advantage of $\mathscr{C}_{4,16}$ using coherent optical OFDM.

3.2 Noncoherent Optical Communications

In wireless optical links [2, 6, 7] and short-haul fiber links used, for example, in data centers [8, 9], there is a need for low-cost and low-complexity solutions. This need has motivated the use of affordable components such as noncoherent optical intensity modulators, direct-detection receivers, and multimode fibers. Communication systems using such components are known as IM/DD systems and will be the focus of our work. As opposed to the coherent systems discussed in Sec. 2.2, the noncoherent optical transmitters and receivers have

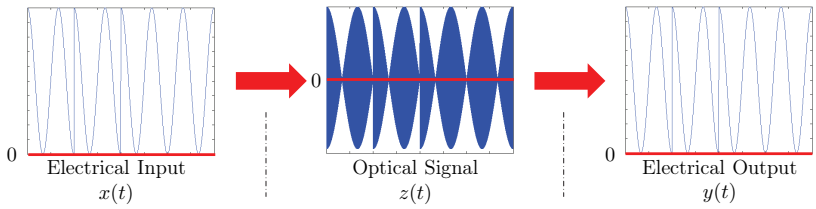

Figure 3.3: Biased BPSK over an IM/DD channel. The waveforms $x(t)$, $z(t)$, and $y(t)$ are described below.

no access to the optical carrier's phase. Therefore, the information is encoded on the intensity of the optical carrier, i.e., the square of the optical amplitude, and the square of the envelope of the received signal is detected at the receiver. The intensity of the optical carrier is, at all time instances, real and nonnegative. This nonnegativity constraint makes the design of IM/DD signaling schemes with good power and spectral characteristics challenging [6, 7, 13, 63], [Paper C]. The common modulation formats optimized for coherent optical communications or for the conventional electrical AWGN channel are in general not applicable to IM/DD.

Figure 3.2 depicts the passband schematic of an IM/DD system. It consists of a light source such as a laser diode that produces light whose intensity is proportional to the input electrical signal. At the receiver, a photodetector outputs an electrical signal proportional to the optical intensity. In [64], a 40 Gbit/s VCSEL-based optical link with an OOK modulation format was demonstrated over 50 m of MMF, and in [45], a 56.1 Gbit/s link was demonstrated in the back-to-back case, i.e., with a short MMF patch cord in order to eliminate the impact of propagation over longer distances. Advances at the hardware level help in increasing the bit rates and/or the transmission reach [11, 65]. Another way to improve the performance is by adopting power-efficient multilevel modulation formats. Since the optical carrier phase cannot be used to carry information, resorting to M-PAM is a natural low-complexity way of improving the spectral efficiency beyond that of the widespread OOK. The M-PAM for IM/DD channels is different from the conventional PAM since no negative amplitudes can be used [6, Eq. (5.8)]. In [66, 67], 4-PAM was experimentally demonstrated over a plastic optical fiber link.

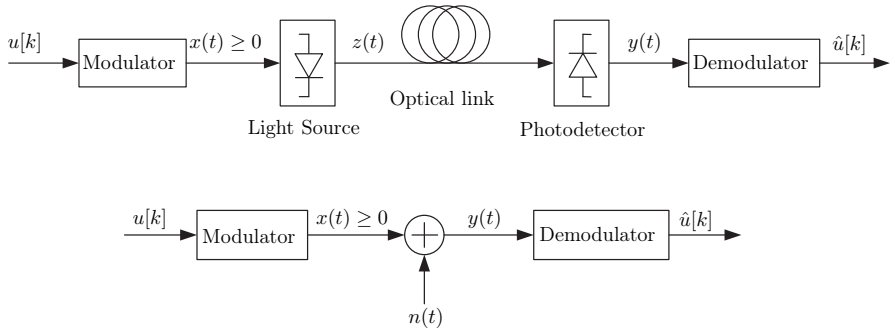

Figure 3.4: Passband transceiver of IM/DD systems (top). Baseband transceiver with constrained-input Gaussian channel (bottom).

Figure 3.2 also shows that any nonnegative electrical waveform can be communicated successfully over an IM/DD link. This implies that if the information to be transmitted is modulated on an electrical subcarrier using any M-level modulation format, it can be transmitted on an IM/DD link after adding a DC bias to ensure its nonnegativity. In this way, the subcarrier amplitude and phase that carry the information can be retrieved at the receiver. This concept is known as *subcarrier modulation* and was originally described in the wireless infrared communications context [6, Ch. 5]. SCM enables the design of modulation formats that are more power efficient than M-PAM. Figure 3.3 shows an example of SCM where the information is modulated on an electrical subcarrier using BPSK. The input to the light source is the electrical subcarrier signal, which is DC biased to become nonnegative. The intensity of the optical signal carries the electrical amplitude and phase. At the receiver, the photodetector, which acts as a square-law detector, puts out the transmitted electrical signal where the electrical amplitude and phase are preserved. This will be followed by a BPSK demodulator to extract the transmitted information bits.

The passband transceiver for IM/DD systems is shown in Fig. 3.4 (top). It consists of a modulator that maps the symbol $u[k]$ at instant k to a waveform belonging to the signaling set $S = \{s_0(t), s_1(t), \ldots, s_{M-1}(t)\}$, where M is the size of the signaling set. The generated

waveform

$$x(t) = \sum_{k=-\infty}^{\infty} s_{u[k]}(t - kT_s), \tag{3.1}$$

where $u[k]$ is an ergodic process uniformly distributed over $\{0, 1, \ldots, M-1\}$ and T_s is the symbol period, is constrained to being real and nonnegative. The baseband signal $x(t)$ is composed of waveforms belonging to S that are shifted by multiples of T_s. This nonnegative waveform $x(t)$ directly modulates a light source, such as a laser diode. Therefore, $x(t)$ is proportional to the square of the envelope, i.e., the intensity, of the passband optical signal

$$z(t) = \sqrt{2cx(t)}\cos(2\pi f_o t + \theta(t)), \tag{3.2}$$

where c represents the electro-optical conversion factor in watts per ampere (W/A) [68–70], f_o is the optical carrier frequency, and $\theta(t)$ is a random phase, uniformly distributed in $[0, 2\pi)$ and slowly varying with t. The optical signal propagates through the optical medium depicted as an optical fiber in Fig. 3.4 (top), which could be a free-space optical link in other applications. At the receiver, the photodetector detects the power of $z(t)$ and outputs $y(t)$. The demodulator with input $y(t)$ is a correlator or matched filter receiver with a minimum-distance detector, i.e., it minimizes the symbol error rate at a given SNR [30, Sec. 4.1]. Its output is $\hat{u}[k]$, the symbol that was most likely sent.

In the absence of optical amplification, the dominant channel impairment in optical IM/DD systems is the thermal noise from the photodetector [71], [3, p. 155]. Therefore, the received electrical signal can be written as

$$\begin{aligned} y(t) &= \mathbb{L}\{rz^2(t)\} + n(t) \\ &= rcx(t) + n(t), \end{aligned} \tag{3.3}$$

where $\mathbb{L}\{\cdot\}$ denotes a unit-gain low-pass filter that cancels the signal alias at twice the carrier frequency, r is the responsivity of the photodetector in A/W, and $n(t)$ is a zero-mean Gaussian process with double-sided power spectral density $N_0/2$. Other noise sources such as shot noise and relative intensity noise can be modeled by a Gaussian distribution, however, the variance of the distribution is dependent on the signal power. Without loss of generality, we set $rc = 1$,

which yields the simplified baseband model in Fig. 3.4 (bottom). The channel response is assumed to be ideal, thus nondistorting in the frequency range of interest. This is to rule out the effect of the channel on the design of modulation formats. This baseband model has been extensively studied in the optical communications context, since it serves as a good model for IM/DD systems without optical amplification [6, Ch. 5], [7, 12–15], [72, Sec. 11.2.3]. It is different from the conventional AWGN channel in Fig. 2.1 since the input $x(t)$ is constrained to being nonnegative as opposed to the passband signal $v(t)$, which can take on negative values. However, there exists no nonnegativity constraint on the signal $y(t)$. It should be noted that there exists another IM/DD model that is relevant when the dominating noise comes from optical amplifiers and not the receiver [72, Sec. 11.2], [73, 74]. The noise in that model has a noncentral χ^2-distribution and not a Gaussian distribution as in this work.

As in (2.5), the continuous-time channel model in (3.3) can be represented by the discrete-time vector model

$$\mathbf{y}[k] = \mathbf{x}[k] + \mathbf{n}[k], \tag{3.4}$$

where, at instant k, $\mathbf{x}[k] \in \Omega$ is the transmitted vector, and $\mathbf{n}[k]$ is a Gaussian random vector with independent elements, zero mean, and variance $N_0/2$ per dimension. Since $\mathbf{x}[k]$ and $\mathbf{y}[k]$ are both stationary memoryless processes, the argument k will be dropped from now on. All modulation formats for the AWGN or coherent optical channel can be used with IM/DD systems if they are DC biased so that the signal driving the light source is nonnegative.

Various modulation formats for IM/DD channels have been analyzed in [6, Ch. 5] and compared to OOK. This included modulation formats such as M-PAM, M-PPM, and modulation formats such as M-PSK and M-QAM with a constant DC bias. For example, at asymptotically high SNR, single-subcarrier QPSK was shown to have a 1.5 dB average optical power penalty compared to OOK to achieve the same bit error rate. As for the conventional electrical channel, many subcarriers can be superimposed, resulting in an FDM system, referred to as multiple-subcarrier modulation in the wireless infrared context [6, p. 122], and OFDM if the carriers are orthogonal [18, 75, 76]. A real-time OFDM-based VLC system operating at 100 Mbit/s was demonstrated in [77]. In addition, laboratory experiments have recorded throughputs of 800 Mbit/s [78]. However,

MSM was shown to have poor power efficiency compared to single-subcarrier modulation [6, Sec. 5.3.2], [19, 79]. Specifically, Barry showed in [6, Sec. 5.3.2] that the average optical power penalty for multiple-subcarrier M-QAM, in comparison with the single-subcarrier case, is $5 \log_{10} N$ dB, where N is the number of subcarriers. Kang and Hranilovic [80] and You and Kahn [23] proposed techniques to reduce this MSM power penalty.

Hranilovic presented in [13] a signal space model for optical IM/DD channels where different basis functions can be used to construct signaling sets. These basis functions include, for example, the *prolate spheroidal* wave functions, scaled and shifted versions of the *Walsh* functions denoted as adaptively-biased QAM (AB-QAM), and three one-dimensional rectangular pulse-shaped PAM symbols denoted as 3-D PAM. In addition, shaping regions to reduce the average and peak optical power were derived, and the performance of some lattice-based modulation formats, which are the result of intersecting a lattice with the shaping region, was reported in [13]. An interesting question, to be investigated in the next chapter, is whether there exist new modulation formats that perform better on the IM/DD channel than already known ones.

Chapter 4

Subcarrier Modulation

The use of subcarrier modulation on IM/DD channels allows the electrical subcarrier amplitude and phase to convey information, provided that the electrical signal at the input of the light source is nonnegative. One option is that the DC bias required to ensure the nonnegativity of the electrical waveform does not carry information [6, Ch. 5]. An experimental demonstration for single-subcarrier modulation formats was carried out in [20], and a novel transmitter design for subcarrier QPSK and 16-QAM was presented in [21, 81]. The second option is to allow the DC bias to carry information, thus potentially improving the power efficiency. This was studied by varying the DC bias on a symbol-by-symbol basis in [22] and within the symbol interval in [23].

This chapter presents the three-dimensional signal space introduced by Hranilovic [13] for single-subcarrier I/Q modulation formats that are compatible with IM/DD systems. This signal space will be used to design power-efficient modulation formats for uncoded IM/DD systems, with and without confining them to a lattice structure. A two-dimensional signal space for optical IM/DD channels is then introduced. The resulting modulation formats have simpler modulator and demodulator structures than the three-dimensional formats.

4.1 Three-Dimensional Signal Space

Single-subcarrier I/Q modulation formats for IM/DD channels can be portrayed in a three-dimensional signal space spanned by the or-

thonormal basis functions

$$\phi_1(t) = \sqrt{\frac{1}{T_s}}\ \mathrm{rect}\left(\frac{t}{T_s}\right), \tag{4.1}$$

$$\phi_2(t) = \sqrt{\frac{2}{T_s}}\ \cos(2\pi f t)\ \mathrm{rect}\left(\frac{t}{T_s}\right), \tag{4.2}$$

$$\phi_3(t) = \sqrt{\frac{2}{T_s}}\ \sin(2\pi f t)\ \mathrm{rect}\left(\frac{t}{T_s}\right), \tag{4.3}$$

where

$$\mathrm{rect}(t) = \begin{cases} 1, & \text{if } 0 \leq t < 1 \\ 0, & \text{otherwise} \end{cases},$$

and f is the electrical subcarrier frequency [13]. The basis function $\phi_1(t)$ represents the DC bias, whereas $\phi_2(t)$ and $\phi_3(t)$ are the basis functions for the conventional I/Q modulation formats presented in Sec. 2.2 with rectangular pulse shaping. As in [6, pp. 115–116] and [13], we use $f = 1/T_s$, which is the minimum value for which $\phi_1(t)$, $\phi_2(t)$, and $\phi_3(t)$ are orthonormal. These basis functions are depicted in Fig. 4.1. In [13], IM/DD modulation formats based on these three basis functions are referred to as raised-QAM, and in [20] as single-cycle SCM.

The use of rectangular pulse shaping results in time-disjoint pulses, i.e., $s_i(t) = 0$ for $t \notin [0, T_s)$ and $i = 0, 1, \ldots, M-1$. Therefore, the criterion of having $x(t)$ in (3.1) to be nonnegative can be simplified to having each of the signals in S to be nonnegative. Thus, $s_{i,1}$ (the coefficient of $\phi_1(t)$ in (2.2)), for $i = 0, \ldots, M-1$, is chosen such that

$$\min_t s_i(t) \geq 0,$$

which guarantees the nonnegativity of $x(t)$ at all times. Hranilovic defined the admissible region Υ as a confined region in the space spanned by the basis functions, where every point belonging to this region corresponds to a nonnegative waveform [13, Eq. (10)]. Therefore, the constellation Ω is a finite set of points in Υ. The admissible region for single-subcarrier I/Q modulation formats when used on

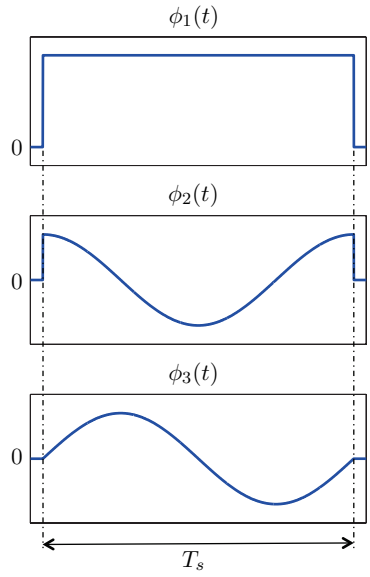

Figure 4.1: Basis functions for single-subcarrier I/Q modulation formats for IM/DD channels.

IM/DD channels is

$$\Upsilon = \{\mathbf{w} \in \mathbb{R}^3 : \min_{t\in[0,T_s)} \sum_{k=1}^{3} w_k \phi_k(t) \geq 0 \}, \tag{4.4}$$

$$= \{\mathbf{w} \in \mathbb{R}^3 : w_1 \geq \sqrt{2(w_2^2 + w_3^2)}\}, \tag{4.5}$$

where $\mathbf{w} = (w_1, w_2, w_3)$. Thus, Υ is a three-dimensional cone with apex angle of $\cos^{-1}(1/3) = 70.528°$ pointing in the dimension spanned by $\phi_1(t)$, with vertex at the origin [2, Fig. 4.2]. Three examples of modulation formats are shown within this cone in Fig. 4.2. The constellation points are the coordinates of the sphere centers, and the diameter of the spheres represents the minimum distance of the constellation. The first modulation format is the one-dimensional nonnegative 4-PAM, whose constellation points are in the $\phi_1(t)$ direction [6, Eq. (5.8)]. The optimal demodulator that minimizes the SER at a given SNR is a one-dimensional demodulator that takes into consideration the amplitude alone, i.e., $\phi_1(t)$. The second modulation format is the conventional 16-QAM, whose constellation points lie on

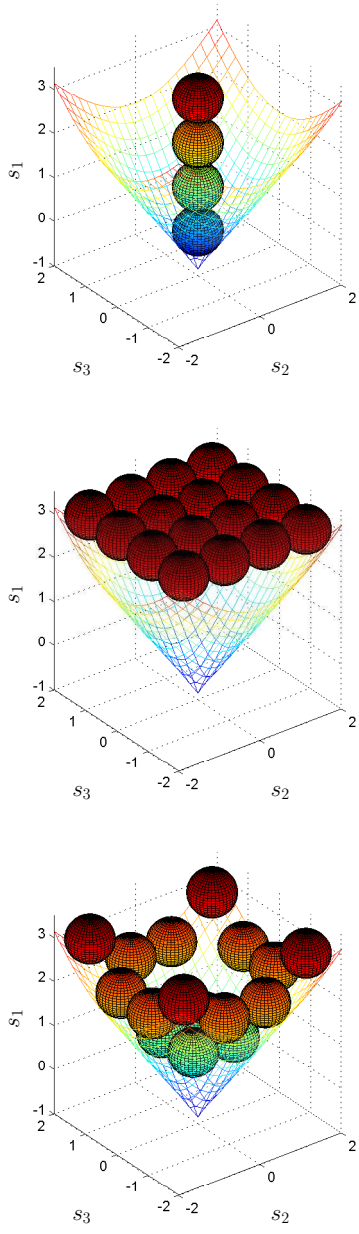

Figure 4.2: 4-PAM (top), 16-QAM (middle), and 16̆-QAM where the DC bias is different for different symbols (bottom). The vertex of the cone is at the origin, however, for illustration purposes, a larger cone is plotted.

three rings with different radii. All the signals of 16-QAM have the same DC bias, chosen sufficiently large so that all the constellation points belong to the admissible region [6, Eq. (5.27)], i.e., they satisfy the nonnegativity constraint of the channel. The optimal demodulator for 16-QAM is the standard I/Q demodulator, which ignores the DC bias or the $\phi_1(t)$ basis function. The last modulation format is a version of 16-QAM denoted as $\breve{1}\breve{6}$-QAM, in which every signal is DC biased with the minimum amount required for it to become nonnegative. This constellation is based on the work in [2, p. 78] and [22], where the DC bias varies on a symbol-by-symbol basis. The coordinates of 16-QAM and $\breve{1}\breve{6}$-QAM are the same in the plane spanned by $\phi_2(t)$ and $\phi_3(t)$. However, the three rings of $\breve{1}\breve{6}$-QAM are not aligned at the same level in the direction spanned by $\phi_1(t)$ since the constellation points lying on each of the three rings require a different DC bias. The standard I/Q demodulator is suboptimal for $\breve{1}\breve{6}$-QAM, however, the performance can be improved by using a three-dimensional demodulator that takes into consideration the three basis functions $\phi_1(t)$, $\phi_2(t)$, and $\phi_3(t)$. The Voronoi diagram of $\breve{1}\breve{6}$-QAM is different from that of 16-QAM with a constant DC bias.

4.2 Two-Dimensional Signal Space

In [Paper E], [Paper F], and [82], we presented a family of two-dimensional signal spaces that can be used to design modulation formats for IM/DD channels. This allows the use of simpler modulator and demodulator structures in comparison to the three-dimensional formats. The signal space is spanned by the two orthonormal basis functions

$$\phi_1(t) = p(t), \tag{4.6}$$

$$\phi_2(t) = H^{\alpha}(t)\, p(t), \tag{4.7}$$

where $p(t)$ is a time-limited unit-energy pulse of duration T_s, nonnegative, and symmetric about $T_s/2$, and for

- $0 \leq \alpha \leq 1$,

$$H^{\alpha}(t) = \begin{cases} A, & 0 \leq t < (1-\alpha)\frac{T_s}{2}, \\ -A\sin(2\pi f(t - T_s/2)), & (1-\alpha)\frac{T_s}{2} \leq t < (1+\alpha)\frac{T_s}{2}, \\ -A, & (1+\alpha)\frac{T_s}{2} \leq t < T_s, \end{cases}$$

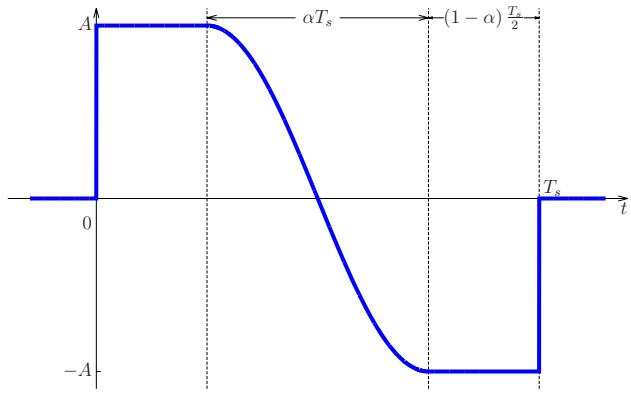

Figure 4.3: $H^{\alpha}(t)$ for $0 \leq \alpha \leq 1$ over $0 \leq t < T_s$. For illustration purposes, $\alpha = 0.5$ in this figure.

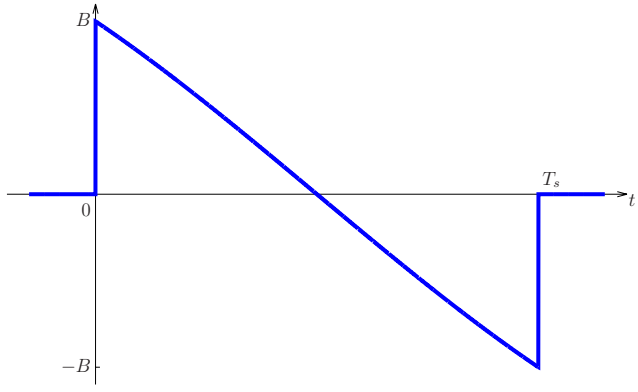

Figure 4.4: $H^{\alpha}(t)$ for $\alpha > 1$ over $0 \leq t < T_s$, where $B = A\sin(\frac{\pi}{2\alpha})$. For illustration purposes, $\alpha = 2.5$ in this figure.

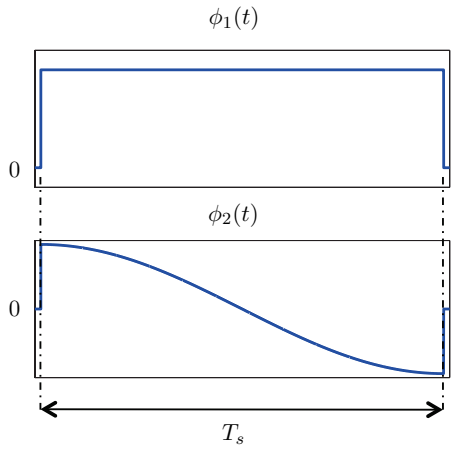

Figure 4.5: Basis functions for the two-dimensional IM/DD signal space for $p(t) = \sqrt{\frac{1}{T_s}}\ \text{rect}\left(\frac{t}{T_s}\right)$ and $\alpha = 1$.

- $\alpha > 1$,

$$H^{\alpha}(t) = -A\sin(2\pi f(t - T_s/2)), \quad 0 \leq t < T_s,$$

where $f = 1/(2\alpha T_s)$ is the subcarrier frequency, and A is chosen such that the energy of $\phi_2(t)$ is unity. This signal is depicted in Figs. 4.3 and 4.4 for $0 \leq \alpha \leq 1$ and $\alpha > 1$, respectively. The choice of α and $p(t)$ has an effect on the spectral efficiency that can be achieved. The signal $H^{\alpha}(t)$ is the first Walsh function for $\alpha = 0$ [2, Sec. 4.2], a half-cycle cosine for $\alpha = 1$ [Paper F], and a sawtooth for $\alpha \to \infty$ [Paper E], [82].

As in Sec. 4.1, an admissible region Υ can be defined to facilitate the design of constellations or signaling sets for IM/DD channels. This region can be expressed as

$$\Upsilon \quad = \quad \{\mathbf{w} \in \mathbb{R}^2 : \min_{t\in[0,T_s)} \sum_{k=1}^{2} w_k \phi_k(t) \geq 0\ \}, \tag{4.8}$$

where $\mathbf{w} = (w_1, w_2)$. This region is a two-dimensional cone with vertex at the origin and an apex angle that depends on the parameter α.

For the case where the pulse shape

$$p(t) = \sqrt{\frac{1}{T_s}}\ \text{rect}\left(\frac{t}{T_s}\right), \tag{4.9}$$

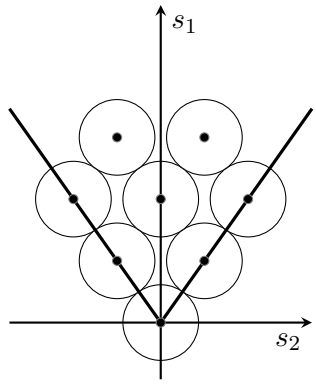

Figure 4.6: An 8-ary two-dimensional constellation portrayed together with the admissible region Υ ($p(t) = \sqrt{\frac{1}{T_s}}$ rect $\left(\frac{t}{T_s}\right)$ and $\alpha = 1$).

the amplitude A that results in a unit-energy $\phi_2(t)$ is

$$A = \begin{cases} \sqrt{2/(2-\alpha)}, & 0 \leq \alpha \leq 1, \\ \sqrt{2/(1-\mathrm{sinc}(1/\alpha))}, & \alpha > 1, \end{cases}$$

where $\mathrm{sinc(x)} = \sin(\pi x)/(\pi x)$. For $\alpha = 1$, the two-dimensional signal space becomes a subspace of the three-dimensional raised-QAM signal space. It is spanned by the two basis functions in (4.1) and (4.2). However, the electrical subcarrier frequency is $f = 1/2T_s$ as opposed to $f = 1/T_s$ for the raised-QAM signal space, as shown in Fig. 4.5 [Paper F], [83, 84]. The admissible region

$$\Upsilon \quad = \quad \{\mathbf{w} \in \mathbb{R}^2 : w_1 \geq \sqrt{2}\,|w_2|\} \tag{4.10}$$

is a two-dimensional cone with vertex at the origin, an apex angle of $\cos^{-1}(1/3) = 70.528°$, and an opening in the dimension spanned by $\phi_1(t)$. By sweeping α from 0 to ∞, the apex angle of the cone changes from 90° to 60°. Figure 4.6 portrays an 8-ary two-dimensional constellation with the admissible region which guarantees that the constellation points belonging to it correspond to nonnegative waveforms. The constellation points are regarded as the centers of circles with diameters equal to the minimum distance of the constellation.

4.3 Figures of Merit

The power and spectral measures used to assess the performance of previously known and newly obtained modulation formats in [Paper A], [Paper C], [Paper E], and [Paper F] are described below.

4.3.1 Power Measures

Unlike the conventional electrical AWGN channel where the two standard power performance measures are the average and peak electrical power, three important performance measures for IM/DD channels can be extracted from the baseband and passband models in Fig. 3.4. The first entity is the average electrical power defined as

$$\bar{P}_e = \lim_{T\to\infty} \frac{1}{2T} \int_{-T}^{T} x^2(t)\,\mathrm{d}t,$$

which for any basis functions can be simplified to

$$\bar{P}_e = \frac{E_s}{T_s} = \frac{1}{T_s}\,\mathbb{E}[\|\mathbf{s}_I\|^2], \tag{4.11}$$

where E_s is the average energy of the constellation, $\mathbb{E}[\cdot]$ is the expected value, and I is a random variable uniformly distributed over $\{0, 1, \ldots, M-1\}$. This entity is an important figure of merit for assessing the performance of digital and wireless communication systems [30, p. 40]. Therefore, it is relevant for IM/DD systems for compatibility with classical methods and results [74, 85]. In addition, it helps in quantifying the impact of relative intensity noise (RIN) in fiber-optical links [68], and in assessing the power consumption of optical systems [24].

The second measure is the average optical power $\bar{P}_o$, which has been studied in [6, 7, 12–14] for the wireless optical channel. Limitations are set on $\bar{P}_o$ for skin- and eye-safety standards to be met. In fiber-optic communications, this entity can be used to quantify the impact of shot noise on the performance [68, p. 20]. It is defined as

$$\bar{P}_o = \lim_{T\to\infty} \frac{1}{2T} \int_{-T}^{T} z^2(t)\,\mathrm{d}t = \lim_{T\to\infty} \frac{c}{2T} \int_{-T}^{T} x(t)\,\mathrm{d}t.$$

This measure depends solely on the DC bias required to make the signals nonnegative and can be represented in terms of the symbol

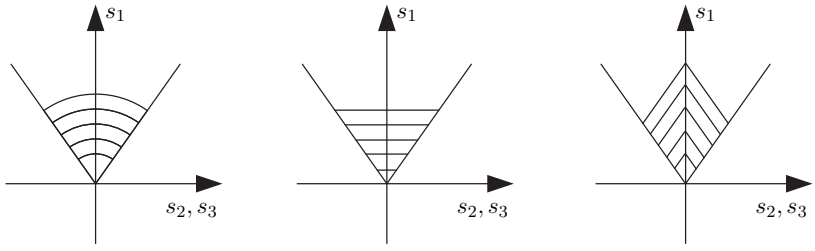

Figure 4.7: (left to right): Contours of equal $\bar{P}_e$, $\bar{P}_o$, and $\hat{P}_o$.

period and constellation geometry as [12, 13]

$$\bar{P}_o = \frac{c}{\sqrt{T_s}} \, \mathbb{E}[s_{I,1}], \tag{4.12}$$

regardless of $\phi_2(t), \ldots, \phi_N(t)$.

The third measure is the peak optical power defined as

$$\begin{aligned} \hat{P}_o &= \max_t \mathbb{L}\{z^2(t)\} && (4.13)\\ &= \max_t \frac{z^2(t)}{2} && (4.14)\\ &= c \max_t x(t) && (4.15)\\ &= c \max_{i,t} s_i(t), && (4.16) \end{aligned}$$

where (4.16) is valid for the time-disjoint signaling considered in this work. It is relevant for investigations of tolerance against the nonlinear behavior of transmitting and receiving hardware in communication systems [13, 25, 70, 86, 87] and has been studied in [13, 14] and [Paper A]. The peak electrical power $\hat{P}_e$ is directly related to $\hat{P}_o$ by

$$\hat{P}_e = \left(\frac{\hat{P}_o}{c} \right)^2,$$

and will not be further considered, since a constellation optimized for $\hat{P}_o$ will automatically be optimized for $\hat{P}_e$ too. A general form for $\hat{P}_o$ as a function of Ω, as in (4.11) and (4.12) for $\bar{P}_e$ and $\bar{P}_o$, does not exist, since $\hat{P}_o$ depends on the exact choice of basis functions. For

the three-dimensional IM/DD basis functions defined in Sec. 4.1, the peak optical power can be expressed as [13, Th. 2]

$$\hat{P}_o = \frac{c}{\sqrt{T_s}} \max_i \left\{ s_{i,1} + \sqrt{2(s_{i,2}^2 + s_{i,3}^2)} \right\}, \tag{4.17}$$

and for the two-dimensional signal space spanned by the basis functions in Fig. 4.5,

$$\hat{P}_o = \frac{c}{\sqrt{T_s}} \max_i \left\{ s_{i,1} + \sqrt{2}\ |s_{i,2}| \right\}, \tag{4.18}$$

for $i = 0, \ldots, M-1$.

Figure 4.7 depicts the contour plots of the three power measures in a two-dimensional signal space together with the admissible region Υ. It can be used as a guideline to design modulation formats suitable for the power constraints that could be present in an IM/DD link.

4.3.2 Spectral Measures

To assess the different modulation formats in the presence of error-correcting codes with performance near capacity, we consider the mutual information [88, Sec. 2.4]

$$I(\mathbf{x};\mathbf{y}) = H(\mathbf{x}) - H(\mathbf{x}|\mathbf{y}) \tag{4.19}$$

as a performance measure. The terms $H(\mathbf{x})$ and $H(\mathbf{x}|\mathbf{y})$ are the entropy of $\mathbf{x}$ and the conditional entropy of $\mathbf{x}$ given the received vector $\mathbf{y}$, averaged over both $\mathbf{x}$ and $\mathbf{y}$. The channel capacity of a discrete memoryless channel is [88, Eq. (7.1)]

$$C = \max_{p(\mathbf{x})} I(\mathbf{x};\mathbf{y}), \tag{4.20}$$

where the maximum is taken over all possible input distributions $p(\mathbf{x})$. For a fixed constellation and distribution, the mutual information gives a lower bound on the channel capacity. In our work, we choose a uniform distribution over the constellation points.

We define $R_s = 1/T_s$ as the symbol rate in symbols per second, $R_b = R_s R$ as the bit rate in bits per second, $E_b = E_s/R$ as the average energy per bit, and R as the number of bits per symbol a modulation format can carry. Furthermore, in order to have a fair comparison of

the bit rates that can be achieved by the different modulation formats in a fixed bandwidth, the spectral efficiency defined as

$$\eta = \frac{R_b}{W} \text{ [bit/s/Hz]}$$

should be taken into account, where W is the baseband bandwidth. In our work, we are interested in two extreme cases: the uncoded system, for which $R = \log_2 M$, and the system with optimal coding, for which $R = I(\mathbf{x}; \mathbf{y})$.

The baseband bandwidth W can be defined as the first null in the spectrum of $x(t)$, i.e., the width of the main lobe, since most of the energy of a signal is contained in this main lobe [6, 63], [Paper C]. Therefore, at the same symbol rate, modulation formats such as OOK and M-PAM, with rectangular pulse shaping, have $W = R_s$, whereas the modulation formats belonging to the single-subcarrier family occupy $W = 2R_s$ [Paper A, Fig. 2]; this is due to the intermediate step of modulating the information on an electrical subcarrier before modulating the optical carrier [6, Ch. 5], [Paper A]. This bandwidth definition does not penalize modulation formats with large side-lobe power. A better bandwidth measure is the fractional power bandwidth W, defined as the width of the smallest frequency interval carrying a certain fraction K of the total power, where $0 < K < 1$. In other words, W is the solution to

$$\frac{\int_{-W}^{W} S_x(f)\,\mathrm{d}f}{\int_{-\infty}^{\infty} S_x(f)\,\mathrm{d}f} = K, \tag{4.21}$$

where $S_x(f)$ is the power spectral density of $x(t)$. This measure accounts for both the discrete and continuous spectrum as in [89]. In [Paper F], W was computed using $K = 0.9$ and $K = 0.99$, which are somewhat arbitrary but commonly used. For IM/DD channels, the discrete spectral component at $f = 0$ (at DC) represents the average optical power of a constellation [2, p. 47]. Specifically, W is reduced if a DC bias is added to the signal. The power spectral density depends on the choice of basis functions, constellation points, and the correlation between symbols. For constellations with uniform probability distribution, $S_x(f)$ can be obtained using [90, Eq. (3.7.6)], which is evaluated using only the Fourier transform of the signals in S.

4.4 Constellation Optimization

As done before for the conventional AWGN channel [35–39], our approach for finding the best constellations can be formulated as a sphere-packing problem with the objective of minimizing a cost function. This cost function depends on the power constraints that might be present in a communication system (see Fig. 4.7). Since the IM/DD channel has a nonnegativity constraint on the signaling set, the admissible region Υ has to be taken into account when designing constellations. Therefore, the spheres, whose centers represent the constellation points, should be packed closely in order to minimize the cost function while fitting in the admissible region. This section presents an example of a 4-ary three-dimensional constellation, followed by a 4-ary two-dimensional constellation, where both are optimized for all power measures.

4.4.1 A Three-Dimensional Modulation Format

Figure 4.8 shows an example of the 4-ary three-dimensional constellation, denoted as $\mathscr{C}_4$, which provides the lowest average electrical, optical, and peak power. The geometry of this constellation is a regular tetrahedron where all the spheres, or the constellation points lying at the vertices of this regular tetrahedron, are equidistant from each other. This constellation is also a subset of the intersection between the admissible region Υ and the face-centered cubic lattice, where the apex of the cone coincides with a lattice point and the lattice is oriented such that two lattice basis vectors lie in the plane spanned by $\phi_2(t)$ and $\phi_3(t)$. It is a remarkable fact that the vertex angle of the tetrahedron, defined as the apex angle of the circumscribed cone, is exactly $\cos^{-1}(1/3)$, which is equal to the apex angle of the admissible region Υ. Thus, $\mathscr{C}_4$ fits Υ snugly, in the sense that all constellation points are equidistant from each other and lie on the boundary of Υ. This modulation format consists of a zero-level signal and a biased ternary PSK constellation [91, 92], and this can be seen in Fig. 4.9. At asymptotically high SNR, the $\mathscr{C}_4$ constellation offers 0.62 dB average optical power gain over OOK.

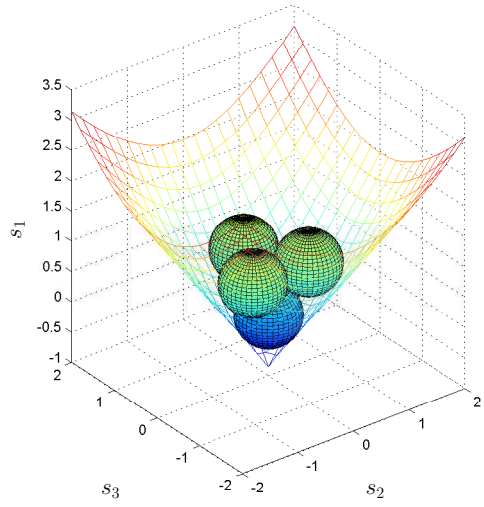

Figure 4.8: The obtained 4-ary three-dimensional constellation ($\mathscr{C}_4$), which is optimized for average electrical, optical, and peak power.

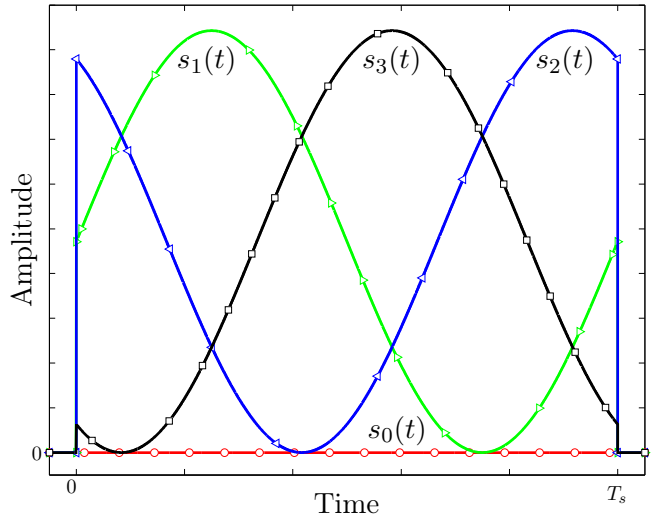

Figure 4.9: The baseband waveforms of $\mathscr{C}_4$ in Fig. 4.8 over one symbol slot.

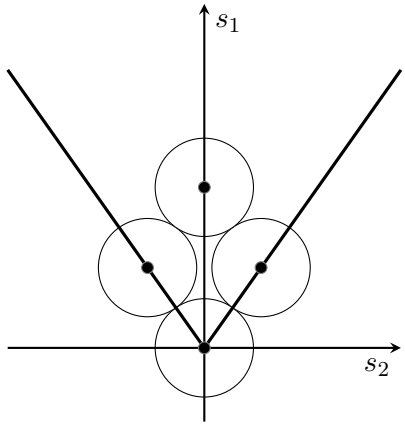

Figure 4.10: The obtained 4-ary two-dimensional constellation ($\mathscr{T}_4$), which is optimized for average electrical, optical, and peak power.

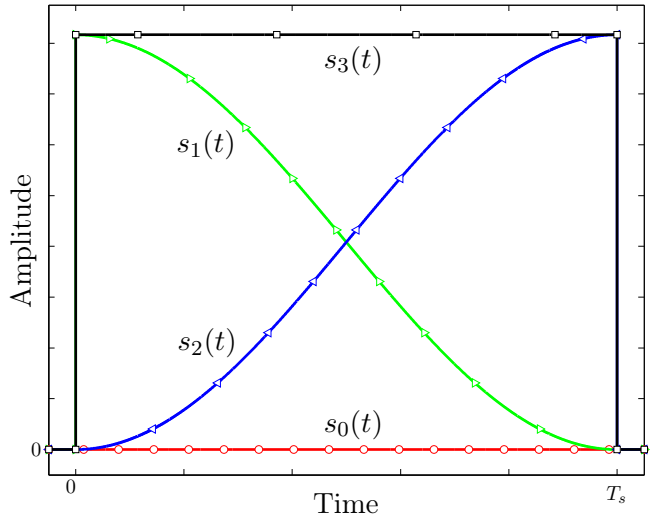

Figure 4.11: The baseband waveforms of $\mathscr{T}_4$ in Fig. 4.10 over one symbol slot.

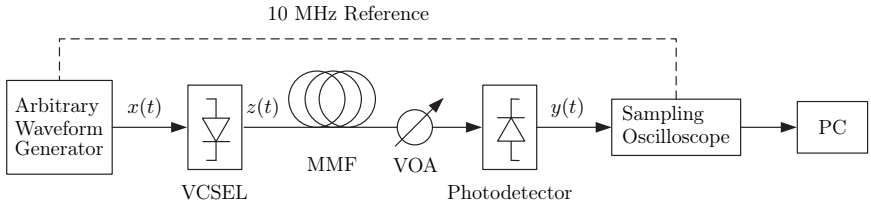

Figure 4.12: Experimental setup.

4.4.2 A Two-Dimensional Modulation Format

Figure 4.10 depicts the 4-ary two-dimensional constellation, denoted as $\mathscr{T}_4$, for rectangular pulse shaping and $\alpha = 1$, optimized for all power measures. This constellation is also a subset of a lattice where the angle between its two basis vectors is $\cos^{-1}(1/3)$, which is the apex angle of the cone. This modulation format is a hybrid between amplitude-shift keying (ASK) and PSK, and the time-domain waveforms are depicted in Fig. 4.11. At asymptotically high SNR, the $\mathscr{T}_4$ constellation has 0.62 dB average optical power penalty over OOK.

In [83, 84], a subcarrier 4-QAM with $f = 1/2T_s$ has been demonstrated over an IM/DD link. This subcarrier 4-QAM, similar to the $\mathscr{T}_4$ modulation format in Fig. 4.10, requires less bandwidth due to the reduced subcarrier frequency compared to single-cycle SCM formats. However, the power efficiency of subcarrier 4-QAM is less than that of $\mathscr{T}_4$. Other hybrids between ASK and PSK have been studied in [60] and [93]; however, such modulation formats do not satisfy the nonnegativity constraint of IM/DD channels.

4.5 Experimental Verification

The theoretical analysis of the newly obtained modulation formats was complemented by an experimental verification [Paper B], [Paper D], [94]. The setup is shown in Fig. 4.12, where the waveforms of the obtained 4- and 8-ary three-dimensional modulation formats have been programmed in an arbitrary waveform generator (AWG). Its output $x(t)$ is fed into a VCSEL, which is a type of low-cost semiconductor laser diode. The generated optical signal $z(t)$ propagates through a multimode fiber, which is followed by a variable optical

attenuator (VOA) to vary the optical power of the propagating signal. At the receiver, a New Focus 1481-S-50 photodetector is used to capture the optical signal, resulting in a current, i.e., the electrical signal $y(t)$, which is proportional to the optical intensity. The electrical signal is then captured with a real-time sampling oscilloscope and processed offline for measurement of the bit and symbol error rates. The offline processing includes computing (2.6) with $\phi_1(t)$, $\phi_2(t)$, and $\phi_3(t)$ given in (4.1)–(4.3), followed by minimum-distance detection.

The modulation formats were operated at a symbol rate of 2.5 Gbaud. Therefore, by choosing the bandwidth of the laser and the photodetector to be around 20 GHz and 25 GHz, respectively, the components were not a limiting factor in the experiment. No amplifier was used after the photodetector, to avoid potential problems with amplifier nonlinearities. In addition, the AWG and the oscilloscope were synchronized to avoid sampling frequency drifts and to remove the need for clock recovery and tracking algorithms, which are outside the scope of this work. Since one of the objectives was to observe the impact of propagation in multimode fibers, equalizers were not used in the setup.

The 4-ary three-dimensional modulation format ($\mathscr{C}_4$) in Fig. 4.8 was transmitted over an MMF with lengths of 800 m and 1000 m. In addition, the back-to-back case with a short MMF patch cord was considered. The experimental bit error rate results confirmed that $\mathscr{C}_4$ is more power efficient in terms of average optical power than other formats with the same spectral efficiency at moderate to high SNR for all the tested fiber lengths (see [Paper B]). The measured gain over OOK is around 0.5 dB at a bit error rate of 10^{-4}, which agrees well with the theoretically derived asymptotic gain of 0.62 dB (see Sec. 4.4.1, [Paper A], and [Paper B]). The experiment also showed that the modulation formats experienced a similar performance penalty due to modal dispersion in the MMF. Modal dispersion occurs since light travels the different modes in an MMF at different velocities. This causes signal broadening and limits the data rates that can be achieved. In Fig. 4.13, the constellation diagram of the received symbols in the back-to-back case is depicted.

In [Paper D], an 8-ary three-dimensional modulation format optimized for average electrical power is demonstrated for the back-to-back case. We chose this constellation instead of the one optimized

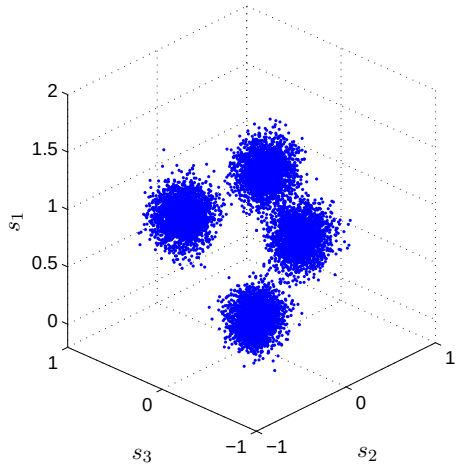

Figure 4.13: Experimental constellation diagram of the 4-ary three-dimensional constellation ($\mathscr{C}_4$) in Fig. 4.8 in the back-to-back case [Paper B].

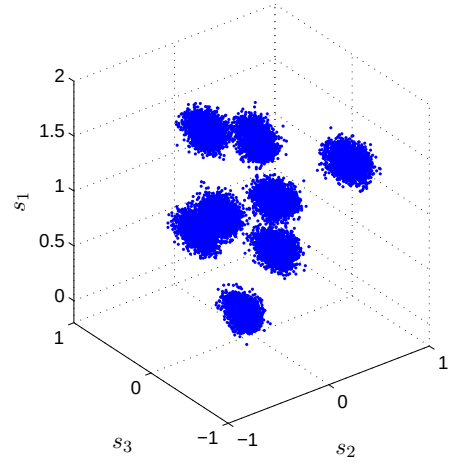

Figure 4.14: Experimental constellation diagram of the 8-ary three-dimensional constellation optimized for average electrical power in the back-to-back case.

for average optical power since it has a simpler and symmetrical structure. At a symbol error rate of 10^{-4}, the experiment showed a gain of around 1 dB in terms of average optical power over previously best known formats with the same spectral efficiency at moderate to high SNR, again supporting the theoretical results in [Paper C]. In Fig. 4.14, the constellation diagram of the received symbols in the back-to-back case is depicted.

The experiments show the implementation feasibility and the gain of the obtained modulation formats over previously best known ones. Therefore, these optimized modulation formats can be a possible option when designing an IM/DD link.

Chapter 5

Contributions

This chapter summarizes the contributions of the appended papers, which fall under the category of designing signaling schemes for optical IM/DD systems.

Paper A: "Power efficient subcarrier modulation for intensity modulated channels"

In this paper, we propose a novel quaternary subcarrier modulation format for IM/DD systems that is a hybrid between on-off keying and ternary phase-shift keying. At asymptotically high signal-to-noise ratios, this hybrid scheme has a 1.2 dB average electrical power gain and 0.6 dB average optical power gain compared to OOK, making it more power efficient than other known formats with a spectral efficiency of 1 bit/s/Hz. However, for systems that are limited by laser nonlinearities, we show that OOK is the best choice.

Paper B: "Experimental comparison of modulation formats in IM/DD links"

This contribution complements the previously obtained theoretical results with an experimental verification. Therefore, we present an experimental comparison of modulation formats over IM/DD systems with a spectral efficiency of 1 bit/s/Hz. This includes OOK, subcarrier QPSK, and the hybrid modulation scheme proposed in [Paper A]. The proposed modulation format is shown to be more power efficient in terms of average optical power compared to the other modulation

formats under study at moderate to high SNR, which is in agreement with the theoretical results. However, the gain comes at the cost of higher transceiver complexity. We also study the impact of propagation in multimode fibers, where the conclusion is that the modulation formats have a similar performance penalty due to the modal dispersion.

Paper C: "Optimizing constellations for single-subcarrier intensity-modulated optical systems"

In this paper, we propose a set of 4-, 8-, and 16-ary single-subcarrier modulation formats for IM/DD systems that are optimized for average electrical, average optical, and peak power. The overall gain compared to the previously best known formats ranges from 0.6 dB to 3 dB in the absence of error-correcting codes. An interesting observation is that modulation formats optimized for peak power perform well in average-power limited systems. We also analyze the obtained modulation formats in terms of mutual information to predict their performance in the presence of strong error-correcting codes. The gain of the obtained formats over previously best known formats ranges from 0.3 dB to 1 dB. Finally, we show numerically and analytically that the optimal modulation formats for reliable transmission in the wideband regime, i.e., at low SNR, have only one nonzero point.

Paper D: "Demonstration of 8-level subcarrier modulation sensitivity improvement in an IM/DD system"

In this paper, we experimentally demonstrate the performance of 8-level subcarrier formats over an IM/DD link. At a symbol error rate of 10^{-4}, the 8-level optimized modulation format obtained in [Paper C] provides a 1 dB average optical power gain over a star-shaped subcarrier 8-QAM with varying DC bias, and a 2 dB improvement over the conventional star-shaped subcarrier 8-QAM with a constant DC bias. This performance improvement is in agreement with the theoretical results.

Paper E: "Modulation method and apparatus for amplitude- or intensity-modulated communication systems"

In this paper, we propose a family of basis functions that can aid in the design of modulation formats that utilize less bandwidth compared to prior art formats, for amplitude- or intensity-modulated communication systems. The resulting signals can be portrayed in a two-dimensional Euclidean space, which in turn leads to a simplified modulator and demodulator structure. Using the signal space and the conical constraint that ensures the nonnegativity of the generated signals, different modulation formats can be designed to suit different constraints that might be present in a communication link.

Paper F: "A two-dimensional signal space for intensity-modulated channels"

In this paper, we present a two-dimensional signal space for optical IM/DD systems. The resulting modulation formats have simpler modulator and demodulator structures than the three-dimensional formats studied before. The uncoded, high-signal-to-noise ratio, power and spectral efficiencies are compared to those of the best known formats. The new two-dimensional modulation formats are superior if the bandwidth is measured as 90% in-band power. This makes them a good choice for single-wavelength optical systems. Existing subcarrier formats are better if the bandwidth is measured as 99% in-band power. Therefore, they are suitable for wavelength-division multiplexing systems where crosstalk between adjacent channels is important.

References

[1] C. E. Shannon, "A mathematical theory of communication," *Bell System Technical Journal*, vol. 27, pp. 379–423 and 623–656, 1948.

[2] S. Hranilovic, *Wireless Optical Communication Systems*. New York: Springer, 2005.

[3] G. P. Agrawal, *Lightwave Technology: Telecommunication Systems*. New Jersey: John Wiley & Sons, Inc., 2005.

[4] K. C. Kao and G. A. Hockham, "Dielectric-fibre surface waveguides for optical frequencies," *Proceedings of the Institution of Electrical Engineers*, vol. 113, no. 7, pp. 1151–1158, Jul. 1966.

[5] D. B. Keck, R. D. Maurer, and P. C. Schultz, "On the ultimate lower limit of attenuation in glass optical waveguides," *Applied Physics Letters*, vol. 22, no. 7, pp. 307–309, Apr. 1973.

[6] J. R. Barry, *Wireless Infrared Communications*. Norwell, MA, USA: Kluwer Academic Publishers, 1994.

[7] J. M. Kahn and J. R. Barry, "Wireless infrared communications," *Proceedings of the IEEE*, vol. 85, no. 2, pp. 265–298, 1997.

[8] S. Randel, F. Breyer, and S. C. J. Lee, "High-speed transmission over multimode optical fibers," in *Proc. Optical Fiber Communication Conference*, 2008, p. OWR2.

[9] D. Molin, G. Kuyt, M. Bigot-Astruc, and P. Sillard, "Recent advances in MMF technology for data networks," in *Proc. Optical Fiber Communication Conference*, 2011, p. OWJ6.

[10] M. A. Taubenblatt, "Optical interconnects for high-performance computing," *Journal of Lightwave Technology*, vol. 30, no. 4, pp. 448–457, Feb. 2012.

[11] A. Larsson, "Advances in VCSELs for communication and sensing," *IEEE Journal of Selected Topics in Quantum Electronics*, vol. 17, no. 6, pp. 1552–1567, Nov./Dec. 2011.

[12] S. Hranilovic and F. R. Kschischang, "Capacity bounds for power- and band-limited optical intensity channels corrupted by Gaussian noise," *IEEE Transactions on Information Theory*, vol. 50, no. 5, pp. 784–795, 2004.

[13] ——, "Optical intensity-modulated direct detection channels: Signal space and lattice codes," *IEEE Transactions on Information Theory*, vol. 49, no. 6, pp. 1385–1399, 2003.

[14] A. A. Farid and S. Hranilovic, "Capacity bounds for wireless optical intensity channels with Gaussian noise," *IEEE Transactions on Information Theory*, vol. 56, no. 12, pp. 6066–6077, 2010.

[15] A. Lapidoth, S. M. Moser, and M. A. Wigger, "On the capacity of free-space optical intensity channels," *IEEE Transactions on Information Theory*, vol. 55, no. 10, pp. 4449–4461, Oct. 2009.

[16] S. Walklin and J. Conradi, "Multilevel signaling for increasing the reach of 10 Gb/s lightwave systems," *Journal of Lightwave Technology*, vol. 17, no. 11, pp. 2235–2248, 1999.

[17] S. Hranilovic, "On the design of bandwidth efficient signalling for indoor wireless optical channels," *International Journal of Communication Systems*, vol. 18, no. 3, pp. 205–228, 2005.

[18] J. Armstrong, "OFDM for optical communications," *Journal of Lightwave Technology*, vol. 27, no. 3, pp. 189–204, Feb. 2009.

[19] J. B. Carruthers and J. M. Kahn, "Multiple-subcarrier modulation for nondirected wireless infrared communication," *IEEE Journal on Selected Areas in Communications*, vol. 14, no. 3, pp. 538–546, Apr. 1996.

[20] A. O. J. Wiberg, B.-E. Olsson, and P. A. Andrekson, "Single cycle subcarrier modulation," in *Proc. Optical Fiber Communication Conference*, 2009, p. OTuE1.

[21] B.-E. Olsson and M. Sköld, "QPSK transmitter based on optical amplitude modulation of electrically generated QPSK signal," in *Proc. Asia Optical Fiber Communication and Optoelectronic Exposition and Conference*, 2008, p. SaA3.

[22] S. Hranilovic and D. A. Johns, "A multilevel modulation scheme for high-speed wireless infrared communications," in *Proc. IEEE International Symposium on Circuits and Systems*, 1999, pp. 338–341.

[23] R. You and J. M. Kahn, "Average power reduction techniques for multiple-subcarrier intensity-modulated optical signals," *IEEE Transactions on Communications*, vol. 49, no. 12, pp. 2164–2171, 2001.

[24] L. P. Chen and K. Y. Lau, "Regime where zero-bias is the low-power solution for digitally modulated laser diodes," *IEEE Photonics Technology Letters*, vol. 8, no. 2, pp. 185–187, 1996.

[25] B. Inan, S. C. J. Lee, S. Randel, I. Neokosmidis, A. M. J. Koonen, and J. W. Walewski, "Impact of LED nonlinearity on discrete multitone modulation," *Journal of Optical Communications and Networking*, vol. 1, no. 5, pp. 439–451, Oct. 2009.

[26] J. G. Proakis, *Digital Communications*, 3rd ed. McGraw-Hill, 1995.

[27] H. Nyquist, "Certain factors affecting telegraph speed," *Bell System Technical Journal*, vol. 3, pp. 324–346, 1924.

[28] R. V. L. Hartley, "Transmission of information," *Bell System Technical Journal*, vol. 7, pp. 535–563, 1928.

[29] N. Wiener, *Extrapolation, Interpolation, and Smoothing of Stationary Time Series with Engineering Applications.* New York: John Wiley & Sons, Inc., 1949 (Reprint of original work published as an MIT Radiation Laboratory Report in 1942).

[30] M. K. Simon, S. M. Hinedi, and W. C. Lindsey, *Digital Communication Techniques: Signal Design and Detection.* Englewood Cliffs, NJ: Prentice-Hall, 1995.

[31] V. A. Kotelnikov, "The theory of optimum noise immunity," Ph.D. dissertation, Molotov Energy Institute, Moscow, 1947.

[32] J. M. Wozencraft and I. M. Jacobs, *Principles of Communication Engineering.* New York: John Wiley & Sons, Inc., 1965.

[33] J. B. Anderson, *Digital Transmission Engineering*, 2nd ed. New Jersey: IEEE Press, 2005.

[34] S. Haykin, *Communication Systems*, 4th ed. New York: John Wiley & Sons, Inc., 2001.

[35] G. Foschini, R. Gitlin, and S. Weinstein, "Optimization of two-dimensional signal constellations in the presence of Gaussian noise," *IEEE Transactions on Communications*, vol. COM-22, no. 1, pp. 28–38, Jan. 1974.

[36] J.-E. Porath and T. Aulin, "Design of multidimensional signal constellations," *IEE Proceedings - Communications*, vol. 150, no. 5, pp. 317–323, Oct. 2003.

[37] N. J. A. Sloane, R. H. Hardin, T. D. S. Duff, and J. H. Conway, "Minimal-energy clusters of hard spheres," *Discrete and Computational Geometry*, vol. 14, no. 3, pp. 237–259, 1995.

[38] R. L. Graham and N. J. A. Sloane, "Penny-packing and two-dimensional codes," *Discrete and Computational Geometry*, vol. 5, no. 1, pp. 1–11, 1990.

[39] E. Agrell and M. Karlsson, "Power-efficient modulation formats in coherent transmission systems," *Journal of Lightwave Technology*, vol. 27, no. 22, pp. 5115–5126, 2009.

[40] G. D. Forney, Jr., "Coset codes–Part I: Introduction and geometrical classification," *IEEE Transactions on Information Theory*, vol. 34, no. 5, pp. 1123–1151, 1988.

[41] G. D. Forney, Jr. and L.-F. Wei, "Multidimensional constellations–Part I. Introduction, figures of merit, and generalized cross constellations," *IEEE Journal on Selected Areas in Communications*, vol. 7, no. 6, pp. 877–892, 1989.

[42] J. H. Conway and N. J. A. Sloane, *Sphere Packings, Lattices and Groups*, 3rd ed. New York: Springer-Verlag, 1999.

[43] E. Specht, "The best known packings of equal circles in the unit circle," 2009. [Online]. Available: http://hydra.nat.uni-magdeburg.de/packing/cci/cci.html

[44] M. Karlsson and E. Agrell, "Power-efficient modulation schemes," in *Impact of Nonlinearities on Fiber Optic Communications*, S. Kumar, Ed. Springer, 2011, ch. 5, pp. 219–252.

[45] D. M. Kuchta, C. L. Schow, A. V. Rylyakov, J. E. Proesel, F. E. Doany, C. Baks, B. H. Hamel-Bissell, C. Kocot, L. Graham, R. Johnson, G. Landry, E. Shaw, A. MacInnes, and J. Tatum, "A 56.1Gb/s NRZ modulated 850nm VCSEL-based optical link," in *Proc. Optical Fiber Communication Conference*, 2013, paper OW1B.5.

[46] F. R. Gfeller and U. Bapst, "Wireless in-house data communication via diffuse infrared radiation," *Proceedings of the IEEE*, vol. 67, no. 11, pp. 1474–1486, Nov. 1979.

[47] M. Kavehrad, "Sustainable energy-efficient wireless applications using light," *IEEE Communications Magazine*, vol. 48, no. 12, pp. 66–73, Dec. 2010.

[48] K.-D. Langer, J. Grubor, O. Bouchet, M. El Tabach, J. W. Walewski, S. Randel, M. Franke, S. Nerreter, D. C. O'Brien, G. E. Faulkner, I. Neokosmidis, G. Ntogari, and M. Wolf, "Optical wireless communications for broadband access in home area networks," in *Proc. International Conference on Transparent Optical Networks*, 2008, pp. 149–154.

[49] Z. Ghassemlooy, "OLED-based visible light communications," in *Proc. IEEE Photonics Society Summer Topical Meetings*, 2012, paper TuB2.3.

[50] J. Vučić and K.-D. Langer, "High-speed visible light communications: State-of-the-art," in *Proc. Optical Fiber Communication Conference*, 2012, paper OTh3G.3.

[51] S. Betti, F. Curti, G. De Marchis, and E. Iannone, "Exploiting fibre optics transmission capacity: 4-quadrature multilevel signalling," *Electronics Letters*, vol. 26, no. 14, pp. 992–993, Jul. 1990.

[52] ——, "A novel multilevel coherent optical system: 4-quadrature signaling," *Journal of Lightwave Technology*, vol. 9, no. 4, pp. 514–523, Apr. 1991.

[53] S. Betti, G. De Marchis, E. Iannone, and P. Lazzaro, "Homodyne optical coherent systems based on polarization modulation," *Journal of Lightwave Technology*, vol. 9, no. 10, pp. 1314–1320, Oct. 1991.

[54] R. Cusani, E. Iannone, A. M. Salonico, and M. Todaro, "An efficient multilevel coherent optical system: M-4Q-QAM," *Journal of Lightwave Technology*, vol. 10, no. 6, pp. 777–786, Jun. 1992.

[55] H. Sun, K.-T. Wu, and K. Roberts, "Real-time measurements of a 40 Gb/s coherent system," *Optics Express*, vol. 16, no. 2, pp. 873–879, Jan. 2008.

[56] M. Seimetz, "Multi-format transmitters for coherent optical M-PSK and M-QAM transmission," in *Proc. 7th International Conference on Transparent Optical Networks*, 2005, pp. 225–229.

[57] J. P. Gordon, L. R. Walker, and W. H. Louisell, "Quantum statistics of masers and attenuators," *Physical Review*, vol. 130, no. 2, pp. 806–812, Apr. 1963.

[58] J. M. Kahn and K.-P. Ho, "Spectral efficiency limits and modulation/detection techniques for DWDM systems," *IEEE Journal of Selected Topics in Quantum Electronics*, vol. 10, no. 2, pp. 259–272, Mar./Apr. 2004.

[59] E. Ip, A. P. T. Lau, D. J. F. Barros, and J. M. Kahn, "Coherent detection in optical fiber systems." *Optics Express*, vol. 16, no. 2, pp. 753–791, Jan. 2008.

[60] R.-J. Essiambre, G. Kramer, P. J. Winzer, G. J. Foschini, and B. Goebel, "Capacity limits of optical fiber networks," *Journal of Lightwave Technology*, vol. 28, no. 4, pp. 662–701, Feb. 2010.

[61] M. Karlsson and E. Agrell, "Four-dimensional optimized constellations for coherent optical transmission systems," in *Proc. European Conference and Exhibition on Optical Communication*, Sep. 2010, p. We8C3.

[62] J. Karout, X. Liu, S. Chandrasekhar, E. Agrell, M. Karlsson, and R.-J. Essiambre, "Experimental demonstration of an optimized 16-ary four-dimensional modulation format using opti-

cal OFDM," in *Proc. Optical Fiber Communication Conference*, 2013, paper OW3B.4.

[63] J. Karout, E. Agrell, K. Szczerba, and M. Karlsson, "Designing power-efficient modulation formats for noncoherent optical systems," in *Proc. IEEE Global Communications Conference*, 2011.

[64] P. Wolf, P. Moser, G. Larisch, H. Li, J. A. Lott, and D. Bimberg, "Energy efficient 40 Gbit/s transmission with 850 nm VCSELs at 108 fJ/bit dissipated heat," *Electronics Letters*, vol. 49, no. 10, May 2013.

[65] R. Safaisini, K. Szczerba, P. Westbergh, E. Haglund, B. Kögel, J. S. Gustavsson, M. Karlsson, P. Andrekson, and A. Larsson, "High-speed 850 nm quasi-single-mode VCSELs for extended-reach optical interconnects," *Journal of Optical Communications and Networking*, vol. 5, no. 7, pp. 686–695, Jul. 2013.

[66] F. Breyer, S. C. J. Lee, S. Randel, and N. Hanik, "PAM-4 signalling for gigabit transmission over standard step-index plastic optical fibre using light emitting diodes," in *Proc. European Conference and Exhibition on Optical Communication*, 2008, p. We2A3.

[67] ——, "Comparison of OOK- and PAM-4 modulation for 10 Gbit/s transmission over up to 300 m polymer optical fiber," in *Proc. Optical Fiber Communication Conference*, 2008, p. OWB5.

[68] C. Cox and W. S. C. Chang, "Figures of merit and performance analysis of photonic microwave links," in *RF Photonic Technology in Optical Fiber Links*, W. S. C. Chang, Ed. Cambridge University Press, 2002, ch. 1, pp. 1–33.

[69] P. Westbergh, J. S. Gustavsson, Å. Haglund, A. Larsson, F. Hopfer, G. Fiol, D. Bimberg, and A. Joel, "32 Gbit/s multimode fibre transmission using high-speed, low current density 850 nm VCSEL," *Electronics Letters*, vol. 45, no. 7, pp. 366–368, 2009.

[70] L. A. Coldren and E. R. Hegblom, "Fundamental issues in VCSEL design," in *Vertical-Cavity Surface-Emitting Lasers: Design,*

Fabrication, Characterization, and Applications, C. W. Wilmsen, H. Temkin, and L. A. Coldren, Eds. Cambridge University Press, 1999, ch. 2, pp. 32–67.

[71] W. Mao and J. M. Kahn, "Lattice codes for amplified direct-detection optical systems," *IEEE Transactions on Communications*, vol. 56, no. 7, pp. 1137–1145, 2008.

[72] K.-P. Ho, *Phase-Modulated Optical Communication Systems*. New York: Springer, 2005.

[73] B. Goebel, R.-J. Essiambre, G. Kramer, P. J. Winzer, and N. Hanik, "Calculation of mutual information for partially coherent Gaussian channels with applications to fiber optics," *IEEE Transactions on Information Theory*, vol. 57, no. 9, pp. 5720–5736, Sep. 2011.

[74] K.-P. Ho, "Exact evaluation of the capacity for intensity-modulated direct-detection channels with optical amplifier noises," *IEEE Photonics Technology Letters*, vol. 17, no. 4, pp. 858–860, Apr. 2005.

[75] S. C. J. Lee, F. Breyer, S. Randel, H. P. A. van den Boom, and A. M. J. Koonen, "High-speed transmission over multimode fiber using discrete multitone modulation," *Journal of Optical Networking*, vol. 7, no. 2, pp. 183–196, Feb. 2008.

[76] S. Dimitrov, S. Sinanovic, and H. Haas, "Signal shaping and modulation for optical wireless communication," *Journal of Lightwave Technology*, vol. 30, no. 9, pp. 1319–1328, May 2012.

[77] K.-D. Langer, J. Vučić, C. Kottke, L. Fernández, K. Habel, A. Paraskevopoulos, M. Wendl, and V. Markov, "Exploring the potentials of optical-wireless communication using white LEDs," in *Proc. International Conference on Transparent Optical Networks*, 2011, paper Tu.D5.2.

[78] J. Vučić, C. Kottke, K. Habel, and K.-D. Langer, "803 Mbit/s visible light WDM link based on DMT modulation of a single RGB LED luminary," in *Proc. Optical Fiber Communication Conference*, 2011, paper OWB6.

[79] S. Randel, F. Breyer, S. C. J. Lee, and J. W. Walewski, "Advanced modulation schemes for short-range optical communications," *IEEE Journal of Selected Topics in Quantum Electronics*, vol. 16, no. 5, pp. 1280–1289, Sep./Oct. 2010.

[80] W. Kang and S. Hranilovic, "Optical power reduction for multiple-subcarrier modulated indoor wireless optical channels," in *Proc. IEEE International Conference on Communications*, 2006, pp. 2743–2748.

[81] B.-E. Olsson and A. Alping, "Electro-optical subcarrier modulation transmitter for 100 GbE DWDM transport," in *Proc. Asia Optical Fiber Communication and Optoelectronic Exposition and Conference*, 2008, p. SaF3.

[82] J. Karout, G. Kramer, F. R. Kschischang, and E. Agrell, "Modulation method and apparatus for amplitude- or intensity-modulated communication systems," U.S. Patent Application No. 13/491,655 (filing date Jun. 8, 2012).

[83] T. T. Pham, R. Rodes Lopez, J. M. Estaran Tolosa, J. B. Jensen, and I. Tafur Monroy, "Half-cycle modulation for VCSEL based 6-Gbaud 4-QAM transmission over 1 km multimode fibre link," *Electronics Letters*, vol. 48, no. 17, pp. 1074–1076, Aug. 2012.

[84] T. T. Pham, R. Rodes Lopez, J. B. Jensen, C. J. Chang-Hasnain, and I. Tafur Monroy, "Sub-cycle QAM modulation for VCSEL-based optical fiber links," *Optics Express*, vol. 21, no. 2, pp. 1830–1839, Jan. 2013.

[85] M. S. Moreolo, R. Muñoz, and G. Junyent, "Novel power efficient optical OFDM based on Hartley transform for intensity-modulated direct-detection systems," *Journal of Lightwave Technology*, vol. 28, no. 5, pp. 798–805, Mar. 2010.

[86] H. Elgala, R. Mesleh, and H. Haas, "An LED model for intensity-modulated optical communication systems," *IEEE Photonics Technology Letters*, vol. 22, no. 11, pp. 835–837, Jun. 2010.

[87] ——, "A study of LED nonlinearity effects on optical wireless transmission using OFDM," in *Proc. Wireless and Optical Communications Networks*, 2009, pp. 388–392.

[88] T. M. Cover and J. A. Thomas, *Elements of Information Theory*, 2nd ed. New Jersey: John Wiley & Sons, Inc., 2006.

[89] T. Aulin and C.-E. W. Sundberg, "Continuous phase modulation—Part I: Full response signaling," *IEEE Transactions on Communications*, vol. COM-29, no. 3, pp. 196–209, Mar. 1981.

[90] S. G. Wilson, *Digital Modulation and Coding*. New Jersey: Prentice-Hall, 1996.

[91] J. R. Pierce, "Comparison of three-phase modulation with two-phase and four-phase modulation," *IEEE Transactions on Communications*, vol. COM-28, no. 7, pp. 1098–1099, 1980.

[92] N. Ekanayake and T. T. Tjhung, "On ternary phase-shift keyed signaling," *IEEE Transactions on Information Theory*, vol. IT-28, no. 4, pp. 658–660, Jul. 1982.

[93] M. C. Gursoy, "Error rate analysis for peaky signaling over fading channels," *IEEE Transactions on Communications*, vol. 57, no. 9, pp. 2546–2550, Sep. 2009.

[94] K. Szczerba, J. Karout, M. Karlsson, P. Andrekson, and E. Agrell, "Optimized lattice-based 16-level subcarrier modulation for IM/DD systems," in *Proc. European Conference and Exhibition on Optical Communication*, 2012.